Stationary flows and periodic dynamics of binary mixtures in tall laterally heated slots

Juan Sánchez Umbría and Marta Net

Abstract The steady and oscillatory dynamics of binary fluids contained in slots heated by the side is studied by using continuation methods, and stability analysis. The bifurcation points on the branches of solutions are determined with precision by calculating their spectra for a large range of Rayleigh numbers. It will be seen that continuation and stability methods are a powerful tool to analyze the origin of the hydrodynamic instabilities leading to steady and time periodic flows, and their dynamics. The role played by the shear stresses of the steady field, and the solutal and thermal buoyancies, at the onset of the oscillations is studied by means of the energy equation of the perturbations. With the parameters used, it is found that the shear is always the main responsible for the instabilities, and that the work done by the two buoyancies can even help to stabilize the fluid. The results also show that binary mixtures of Prandtl number order one, like pure gases, present multiple stable periodic flows coexisting in the same range of parameters, since several unstable leading multipliers remain attached to the unit circle and go back into it. However, at lower Prandtl numbers only the first branch of periodic orbits bifurcating directly from the steady state is found to be stable, because some of the unstable multipliers of the other branches quickly increase their modulus and never re-enter the unit circle.

Key words: Continuation methods, Stability analysis, Periodic orbits, Binary mixtures, Lateral heating.

Juan Sánchez Umbría
Departament de Física, Universitat Politècnica de Catalunya.
Jordi Girona Salgado 1-3. Campus Nord. Mòdul B4. 08034 Barcelona. Spain, e-mail: juan.j.sanchez@upc.edu

Marta Net
Departament de Física, Universitat Politècnica de Catalunya.
Jordi Girona Salgado 1-3. Campus Nord. Mòdul B4. 08034 Barcelona. Spain, e-mail: marta.net@upc.edu

1 Introduction

1.1 Double-diffusive convection in slots

The thermal convection in rectangular cavities with horizontal heating has received great attention in the past. Among other industrial applications it is worth mentioning the growth of single liquid crystals [30], convective motions must be damped in order to maintain the melt as steady as possible, and to avoid the growth of perturbations leading to transitions to time dependent flows [55]. The knowledge of the properties of the thermosolutal convection in a wide range of Prandtl numbers is also important for getting an optimal performance of the thermoacoustic engines, since the thermal penetration depth is an important factor to take into account in the design of this type of engines. In fact, the best working gases are mixtures of helium and xenon that can reach low Prantl numbers and the highest ratio of specific heats at pressures lower than 4.5 MPa [52]. Other examples are the design of large-scale laser systems in order to minimize the optical distortion due to buoyancy-driven flows [13], and the optimal heating or cooling and isolation of buildings. Despite its importance the number of articles devoted to double-diffusive convection in tall cavities is not as large as that for pure fluids. See for instance Refs. [120, 62, 125, 115, 63, 39, 92, 122, 49, 77], among many others, that study the 2D-approximation. A good review of the state of knowledge in infinite vertical layers, and in three-dimensional convection up to 2010, can be found in the book of M. Lappa [61]. In addition, some new contributions devoted to study the transition to chaos of the three-dimensional convection between two vertical plates have recently appeared [34, 33].

The onset of steady convection of pure fluids of moderate Prandtl number ($\mathrm{Pr} \approx 1$) in tall slots gives rise to a global circulation with hot fluid rising near the heated side, and the internal core remains almost stably stratified. The instability of this state gives rise to trains of waves travelling by the boundary layer, from the middle of the domain to the lids, where they diffuse [125, 122, 123, 77]. Several stable waves of this type coexist at different intervals of the Rayleigh number, Ra, because the unstable Floquet multipliers remain attached to the unit circle, becoming stable at successive Hopf bifurcations before increasing their modulus definitively. The period of the oscillations is of order 10^{-3} in thermal units (d^2/κ). At low Pr the behavior of the flows is completely different. The velocity field of the steady solutions consists of a vertical alignment of vortices turning in the same direction, whose number depends on the length of the box [98]. The changes of the steady and time periodic flows by using Pr as continuation parameter was analyzed in Ref. [98] for a slot of $\Gamma = 8$. It was found that for $0.2 < \mathrm{Pr} < 0.3$ the time periodic flows are slow internal oscillations due to the shear, consistent of transients between the global circulation and the formation of the vortices. These oscillations have periods two orders of magnitude higher than those of the travelling waves. At even lower values of $\mathrm{Pr} \leq 0.1$ secondary vortices appear between the main. At low Ra the work done by the buoyancy force can even help to stabilize the steady flows.

Continuation methods and stability analysis are used in this work to study the behavior of the steady and time periodic flows of binary mixtures contained in a rectangular slot of aspect ratio $\Gamma = 8$, heated by the side, and with adiabatic lids. The parameter is defined as $\Gamma = h/d$, h and d being the height and width of the box, respectively. Double-diffusive convection with Soret effect, and the two buoyancy forces not in balance, is considered. This effect measures the generation of concentration gradients due to the temperature gradients. As far as we know, this general case, has not been studied before. The power of the continuation methods will be used to analyze the oscillatory instabilities, and the periodic flows and their bifurcations, either under a physical point of view, or as a dynamical system. Continuation methods have important advantages versus time-dependent simulations for these types of regimes. The critical parameters corresponding to the threshold are only affected by the truncation error. They are obtained faster than if they are deduced from the transients of the time integrations, specially when oscillatory flows are involved. Another advantage is that the computation of unstable branches of orbits allows to understand more easily the transients among branches, and the origin of the stable quasiperiodic flows found by time evolution [93, 33, 77].

Since the experimental work of J. Lee *et al.* [64] in moderate aspect ratio boxes, doubly diffusive convection was studied numerically by several authors with different boundary conditions for the temperature and the concentration, and non-slip sides. N. Tsitverblit [109] studied numerically the origin and structure of the multiple steady solutions existent for several values of the salinity Rayleigh number, with salted water of Prandlt number $\mathrm{Pr} = 6.7$ as convecting fluid. He showed that they exist as a result of nondegenerate hysteresis points and isolas of asymmetric solutions forming as Ra is increased. A complete study of the convection when a lateral temperature gradient is applied to a motionless liquid layer, which is stably stratified through a constant vertical salinity gradient, was carried out in Ref. [56]. They focussed their objectives in determining the large scale effects that double-diffusive layered structures have on the vertical transport of fluid constituents.

By enforcing equal and opposite thermal and solutal buoyancy forces (buoyancy number $N = -1$) K. Ghorayeb and A. Mojtabi demonstrated that there exist a trivial equilibrium solution, initially linearly stable if the vertical derivatives of the temperature and concentration gradients are imposed to vanish at the lids [41], as it happens for instance in a periodic vertical layer. They calculated the steady states bifurcated from the trivial one for gaseous mixtures of $\mathrm{Pr} = 1$ and Lewis number $\mathrm{Le} > 1$. Their investigations showed that the onset of double diffusive convection corresponds to a transcritical bifurcation point, and that the result is weakly dependent on Le.

The same two-dimensional problem with the constraint $N = -1$ was studied in Refs. [124, 6, 7, 68] with vertical periodic boundary conditions. In the first paper, the calculations of S. Xin *et al.* showed that, with the preceding parameters of the above paragraph and constant temperature and concentration at the sides, the onset of convection corresponds to a subcritical pitchfork bifurcation. The branch of the steady solutions loses stability to waves traveling in the vertical direction via a supercritical drift pitchfork bifurcation. The calculation of the branches of this steady solutions by A. Bergeon and E. Knobloch [6, 7] showed the presence of spa-

tially localized states that the authors linked with the phenomenon of homoclinic snaking. Recently, the same problem, with no net vertical mass flux and Robin boundary conditions for the concentration at the sides, was revisited in Ref. [68]. As in the preceding works, steady localized states organized in 'snakes-and-ladders' were found. In addition, a family of travelling pulses disconnected from all the other known states was obtained. However, waves travelling up or down a sidewall, like in the general case, were obtained by relaxing the balance of horizontal gradients. Secondary bifurcations from these states give rise to spatially modulated travelling states, and to spatially localized travelling pulses. Localized states were also found in Ref. [5] in a three-dimensional box. In this case, two snaking branches of symmetric steady solutions, bifurcating simultaneously from the trivial state, undergo secondary symmetry breaking bifurcations generating secondary snaking branches of localized states.

1.2 Continuation methods for partial differential equations

The study of numerical models in Fluid Mechanics consisted during many years, after the first high speed digital computers became available, in writing and running time evolution codes to explore the dynamics of the resulting discretized systems of partial differential equations (PDEs). Even the computation of steady solutions was performed by letting the system evolve, passing a transient, to reach the equilibria. This was forced by the small size of the computers memories, which prevented in many cases the use of algorithms to solve nonlinear systems of equations. The landmarking and still very good introductory book by P.J. Roache [85] presents the state of the art at that time. Only linear systems of equations are mentioned there, obtained after the discretization by means of finite differences of the stream function equation or in the context of implicit time integration methods. They were solved by direct methods in case of tridiagonal systems or by highly efficient block methods, tensor product methods, Fourier series methods, etc. A review of what was available at that time for this purpose can be found in Ref. [27]. These methods were considered, at that time, to require large storage. Iterative Richardson, Jacobi, Gauss-Seidel, or alternate directions methods were also used and preferred due to the low storage required.

The application of continuation methods in large-scale systems, to study the dependence of equilibria with parameters, started very probably in the field of structural mechanics with the name of *the method of incremental loads* [84]. A one-parameter dependent increasing load was the continuation parameter to reach the final deformation state starting from the unloaded trivial case. The non-linearity comes in this case not necessarily from the constitutive laws, but from the geometry of the structure when the displacements cannot be considered to be very small. Examples of non-trivial curves of solutions with folds can be obtained in the case of shallow domes [121].

In the case of Fluid Mechanics, an early example of the application of continuation methods can be found in Ref. [73] after, but close in time to, the pioneering work by H.B. Keller on the pseudo-arclength method [53]. They studied the Taylor vortices in the Couette-Taylor system, a classical problem consisting in the study of the flow between two coaxial rotating cylinders. There are contributions by several authors to this problem using continuation methods [22, 2], using an initial version of AUTO [23] in the first case. A.K. Cliffe [14, 15] not only computed the dependence of Taylor vortices on the Reynolds number of the inner cylinder, but also tracked saddle-node and pitchfork bifurcations curves, and detected the presence of cusp points. He used the finite elements (FEM) library ENTWIFE, he contributed to develop. This is, as far as we know, the first direct computation of bifurcation loci in a Fluid Mechanics problem.

In all the above mentioned cases the calculations were possible thanks to the sparse structure of the matrices of the linear systems, which allowed using adapted direct solvers. New linear solvers as GMRES and BiCGStab, based on Krylov subspaces [90, 106], allowed the study of larger systems, and using also spectral or pseudo-spectral methods. Inexact Newton-Krylov matrix-free methods [20, 80] have been used to find steady states and traveling waves, and subspace iteration or Arnoldi's methods to study their stability [71, 4, 9, 74, 111, 69, 10, 82, 116, 31, 93]. In the latter case the Krylov subspaces generated during the GMRES iterations can be recycled to obtain information on the stability [37]. Preconditioning is usually needed to overcome the difficulty in achieving fast convergence of these iterative methods when computing equilibria [88, 97].

There are, at least, three freely available software packages for the computation of equilibria of PDEs which allow tracking them and, in the first case, also loci of their generic codimension-one bifurcations. LOCA [91] is a general-purpose package, included in the C++ Trilinos huge library. It is intended for large-scale systems using all the parallelizing tools provided within the Trilinos solvers. Oomph-lib [48] is also a C++ object-oriented, open-source finite-element library for the simulation of multiphysical problems. The Matlab code pde2path [112] is mainly for one and two-dimensional problems since it is based on the FEM toolbox *pdetoolbox*.

More time was needed to see the first attempts to compute other types of invariant objects in an efficient and systematic way. In the case of periodic orbits, the monodromy matrix is no longer sparse, no matter the method used to discretize the system of PDEs. Therefore matrix-free methods are mandatory in the case of large-scale systems. Newton-Picard algorithms were implemented to compute them giving rise to the package PDECONT [70], used also in Ref. [108] for the flow in a lid-driven cavity. The algorithm was based on a previous idea consisting in removing the growth along the unstable directions of an equilibrium during a time integration [105]. Broyden's method was used in Ref. [79] in the study of chemical reactors, and Newton-Krylov techniques were first introduced in Refs. [99, 100]. This latter method has become the standard used by several authors in different applications due to its simplicity and efficiency [114, 28, 42, 82, 117, 118, 45, 36, 77]. An extension of pde2path for the continuation of cycles, by using collocation in time as in AUTO, has been very recently developed. The same technique was also used,

by coupling the generic continuation package Coco [18] to the FEM library COMSOL [17], to study cycles of periodically forced nonlinear models of a beam [32].

An improved algorithm for the continuation of periodic orbits, using multiple shooting and parallelism, was presented in Ref. [95], and applied in Ref. [117] to study acoustic resonances in a thermoacoustic system. The equations of the multiple shooting were solved by Newton-Krylov methods, but it was seen that a direct application, with each partial shoot computed in a different processor, did not provide any substantial speedup. To achieve a linear speedup some kind of preconditioning for the linear systems had to be used. It was shown how this could be done from the information on the stability of nearby periodic orbits. This information is usually available from the continuation and bifurcation analysis, since the stability is computed frequently. Therefore the preconditioner can be obtained at a low extra cost. This idea of using the information on the stability to accelerate the convergence was the key ingredient of the variants of the Picard iteration described in Ref. [105], for equilibria, and in Ref. [70] for the computation of periodic orbits.

More sophisticated computations of invariant objects came later. Newton-Krylov methods for computing invariant tori for large-scale applications were first considered in Ref. [101]. An improved parallel algorithm appeared in Ref. [96]. The idea was to compute a single point on the surface of the two-dimensional torus, or a set of points approximating an arc of the invariant curve on a Poincaré section. The computation of segments of two-dimensional unstable manifolds of periodic orbits was developed in Ref. [113]. The idea was solving a boundary-value problem, introduced in Ref. [57] following the ideas presented in Ref. [58], to compute stable or unstable manifolds of vector fields.

The computation of loci of bifurcations of equilibria in Fluid Mechanics [15] has already been mentioned. The theory on the extended systems used to follow bifurcations of steady states of low-dimensional systems is well developed and can be found, among others, in Refs. [103, 75, 46, 119, 86, 16, 44]. The bordered systems for periodic orbits, based on boundary value problems, are analyzed in Ref. [25]. In this latter case piecewise collocation in time is used instead of shooting methods together with adapted direct linear solvers. The continuation of codimension-one bifurcations of periodic orbits for high-dimensional systems using Newton-Krylov techniques has been developed only recently [76]. It requires integrating up to second order variational equations, but it was shown that for Navier-Stokes equations they do not differ much from the original because only quadratic non-linear terms are present. The thermal convection of a mixture of two fluids in a two-dimensional rectangular box was used as test problem. A non-trivial diagram of periodic orbits was first deployed, by varying only a parameter (the Rayleigh number), and some of the bifurcations found on the main branch of cycles were followed by adding a second parameter (the Prandtl number). Several codimension-two points were found. It was also shown how the boundaries of resonance regions (Arnold's tongues) can also be continued.

The bibliography on generic continuation methods is very extensive. Their development can be followed in Refs. [19, 59, 83, 54, 1, 104, 60, 44, 24, 18]. Some relevant references, in the case of recent applications to large-scale problems, are

[50, 16, 26, 51, 21, 97]. They are always implemented as predictor-corrector methods. A first approximation is first obtained by extrapolation from previous points along the curve of solutions, which is corrected by any variant of Newton's method. As far as know, the only attempt to improve this methodology is described in Ref. [3] were the PAMPAC algorithm is described. It is a parallel method for adapting the step length employing several predictor-corrector sequences of different step lengths, computed concurrently. The algorithm permits intermediate results of correction sequences that have not yet converged to seed new predictions, generating a tree of corrections which branches are spawned or pruned according to the speed of convergence of Newton's method, using a sophisticated algorithm.

In the remaining of the paper, after the introduction, the equations are derived in Sect. 2, and their numerical treatment by Newton-Krylov methods is discussed in Sect. 3, which also includes the checking of the codes. Sect. 4 contains a brief comparison of the steady solutions and time periodic orbits bifurcated and their stability, of a pure fluid and a gaseous binary mixture of the same $\mathrm{Pr} = 0.683$. In Sect. 5 a detailed study of the behavior of the steady and periodic flows bifurcated from the first, for four different binary mixtures of $\mathrm{Pr} < 1$ is undertaken. It includes an analysis of the energetic balances leading to the oscillations. The paper finishes in Sect.6 with the conclusions obtained from the results.

2 Mathematical formulation

The dynamics of binary mixtures filling a slot, Ω, of width d, height h, and aspect ratio $\Gamma = h/d = 8$ is studied. The boundaries are taken non-slip, the vertical sides are maintained at uniform temperatures, and the top and bottom are enforced to be insulating. No mass flux through the boundaries is considered. The fluid is subject to a vertical gravity, $\mathbf{g} = -g\mathbf{j}$, $\mathbf{j}$ being the unit vector pointing upwards. The Boussinesq approximation of the mass, momentum and energy equations is extended to that of the concentration for the denser component of the mixture. Accordingly, the density in the buoyancy force is taken as

$$\rho = \overline{\rho}\left(1 - \alpha(T - \overline{T}) + \beta(C - \overline{C})\right), \tag{1}$$

α and β being the thermal and the solutal expansion coefficients, respectively, measured at the temperature of reference $\overline{T}$ and concentration $\overline{C}$ to which the density is $\overline{\rho}$. They are defined as

$$\alpha = -\frac{1}{\overline{\rho}}\left(\frac{\partial \rho}{\partial T}\right)_{T=\overline{T}} \quad \text{and} \quad \beta = \frac{1}{\overline{\rho}}\left(\frac{\partial \rho}{\partial C}\right)_{C=\overline{C}}. \tag{2}$$

The equations are nondimensionalized by taking d, the difference of temperature between the left and the right sides of Ω, ΔT, and d^2/κ, κ being the thermal diffusivity, as units of longitude, temperature and time, respectively. In addition, the concentration will be rescaled with $-K_T \Delta T/\overline{T}$, in order to help decoupling the

boundary condition of the concentration. In the preceding expression K_T is the thermal diffusion ratio.

Liquid mixtures of ^{3}He-^{4}He that, according to Ref. [107], have $\mathrm{Pr} = 0.707$ and $\mathrm{Le} = 0.076$, of Fe-Si at high temperature and pressure that, based on data extracted from Ref. [81], have $\mathrm{Pr} = 0.046$ and $\mathrm{Le} < 0.01$, and a mixture of $\mathrm{Pr} = 0.1$ and $\mathrm{Le} < 0.05$, taken ad hoc to cover a more complete range of parameters, will be studied. In addition, a gaseous mixture of Ar-CO_2 of $\mathrm{Pr} = 0.683$ and $\mathrm{Le} = 1.085$ will be also analyzed. It is known that in gaseous mixtures the Dufour effect could be relevant [47]. However, for the values of the parameters of the gas mixture selected, Liu and Ahlers showed in Ref [67] that, even with a Dufour coefficient as large as 37.83, the Dufour effect is very small, because, in fact, it depends on products of the parameters. Then the Dufour term will be excluded from the formulation, and only the Soret term will be taken into account.

In non-dimensional units $\Omega = [0,1] \times [0,\Gamma]$. Let x and y be the horizontal and vertical coordinates, respectively. The system is written by splitting the nondimensional temperature and concentration into a linear x-dependent function and their perturbation Θ or Σ as

$$T(x,y,t) = (1-x) + \Theta(x,y,t) \quad \text{and} \tag{3}$$

$$C(x,y,t) = -(1-x) - \Sigma(x,y,t), \tag{4}$$

in order of having homogeneous boundary conditions on the vertical walls. Then the system that describes the problem is

$$\boldsymbol{\nabla} \cdot \mathbf{v} = 0, \tag{5}$$

$$(\partial_t + \mathbf{v} \cdot \boldsymbol{\nabla})\mathbf{v} = -\boldsymbol{\nabla}\Pi + \mathrm{Pr}\Delta\mathbf{v} - \mathrm{Ra}\,\mathrm{Pr}[(1+\mathrm{Se})(x-\Theta) - \mathrm{Se}\,\eta]\mathbf{j}, \tag{6}$$

$$(\partial_t + \mathbf{v} \cdot \boldsymbol{\nabla})\Theta = \Delta\Theta + v_x, \tag{7}$$

$$(\partial_t + \mathbf{v} \cdot \boldsymbol{\nabla})\eta = \mathrm{Le}\Delta\eta - \Delta\Theta, \tag{8}$$

where $\eta = \Sigma - \Theta$, $\mathbf{v} = (v_x, v_y)$ is the velocity field, and Π contains terms coming from the dependence of ρ on T and C, and on the splitting of these magnitudes. The problem depends on four physical parameters, the Rayleigh, Ra, Prandtl, Pr, and Lewis, Le, numbers, and the separation ratio, Se. They are defined as

$$\mathrm{Ra} = \frac{\alpha g \Delta T d^3}{\nu\kappa}, \quad \mathrm{Pr} = \frac{\nu}{\kappa}, \quad \mathrm{Se} = \frac{\beta K_T}{\alpha \overline{T}}, \quad \mathrm{Le} = \frac{D}{\kappa}, \tag{9}$$

ν being the kinematic viscosity, and D the solutal diffusion coefficient. The Rayleigh number will be used as control parameter in the continuation of the branches of solutions.

The boundary conditions considered can be written as

$$\mathbf{v} = \mathbf{0} \text{ on } \partial\Omega, \tag{10}$$

$$\Theta = 0 \text{ on } x = 0,1 \quad \text{and} \quad \partial_y\Theta = 0 \text{ on } y = 0,\Gamma, \tag{11}$$

$$\partial_n\eta = 0 \text{ on } \partial\Omega, \tag{12}$$

where $\partial\Omega$ means the contour of the domain, and ∂_n the normal derivative to any side.

Equations (5)-(12) are rewritten in terms of a stream function, ψ, related with the velocity field by $\mathbf{v} = (\partial_y\psi, -\partial_x\psi)$. They become

$$\partial_t\Delta\psi - J(\psi,\Delta\psi) = \mathrm{Pr}\Delta^2\psi + \mathrm{RaPr}[(1+\mathrm{Se})(1-\partial_x\Theta) - \mathrm{Se}\partial_x\eta)], \tag{13}$$

$$\partial_t\Theta - J(\psi,\Theta) = \Delta\Theta + \partial_y\psi, \tag{14}$$

$$\partial_t\eta - J(\psi,\eta) = \mathrm{Le}\Delta\eta - \Delta\Theta, \tag{15}$$

with $J(f,g) = \partial_x f\partial_y g - \partial_y f\partial_x g$, and the boundary conditions for ψ translate into

$$\psi = \partial_n\psi = 0 \text{ on } \partial\Omega. \tag{16}$$

In this way the incompressibility condition is identically fulfilled, and the number of unknowns is reduced.

Equations (13)-(15) together with boundary conditions (16), (11) and (12) are $\mathbb{Z}_2$-equivariant, i.e. they remain invariant under the change

$$(t,x,y,\psi,\Theta,\eta) \to (t,1-x,\Gamma-y,\psi,-\Theta,-\eta). \tag{17}$$

3 Numerical methods

To obtain the numerical solutions, the functions ψ, Θ and η were approximated by a pseudo-spectral collocation method on a mesh of $n_x \times n_y$ Gauss-Lobatto points. To discretize the system, the spatial operators are transformed into matrices operating on the values of the functions at the collocation mesh points. Their actions are calculated by means of matrix-matrix products using a high-performance implementation of the DGEMM subroutine of the BLAS library (see [43]). The stiff system of ordinary differential equations (ODEs), obtained after the spatial discretization, is integrated by means of fifth order semi-implicit backward-differentiation-extrapolation formulas as described, for instance, in Ref. [35].

The branches of stationary and periodic solutions were calculated by using continuation methods for large-scale dissipative systems, based on the Newton-Krylov techniques proposed, among others, in Refs. [11, 29, 99, 100, 76]. These techniques are summarized in the following paragraphs and subsections.

Consider a general large-scale system of nonlinear equations, depending on a parameter p,

$$H(z,p) = 0, \quad (z,p) \in \mathscr{V} \subset \mathbb{R}^m \times \mathbb{R}, \tag{18}$$

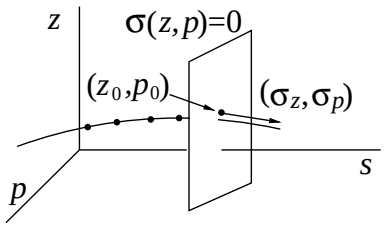

Fig. 1 Scheme of the pseudo-arclength condition taken during the continuation process.

obtained by discretizing a system of PDEs. Several methods are available to track the dependence of its solutions with the parameter p. The pseudo-arclength continuation method is described here. Assume that a curve of solutions and corresponding parameters is written as a function $(z(s), p(s))$ of the arclength s. Then, given an initial solution $(z(0), p(0))$, advancing along the curve can be accomplished by the combination of two stages, a predictor step in which an initial guess to a new point on the curve is computed by extrapolation from the previous solutions (see Fig. 1), and a corrector step in which the prediction is refined. In order to determine simultaneously a unique pair (z, p), the equation

$$\sigma(z,p) = \langle \sigma_z, z - z_0 \rangle + \sigma_p(p - p_0) = 0 \tag{19}$$

is added to the system (18), (z_0, p_0) and (σ_z, σ_p) being the predictions of the new point and the tangent to the curve of solutions, respectively. The hyperplane $\sigma(z,p) = 0$ will cut it transversely if the prediction is not far away from the previous point. This algorithm allows passing turning points if they are present. Therefore the system that determines a unique solution, (z, p), is

$$\begin{aligned} H(z,p) &= 0, \\ \sigma(z,p) &= 0. \end{aligned}$$

These nonlinear systems are usually solved by Newton's method. Starting from the initial prediction (z_0, p_0) a sequence of approximations

$$(z_{i+1}, p_{i+1}) = (z_i, p_i) + (\Delta z_i, \Delta p_i),$$

are computed, where $(\Delta z_i, \Delta p_i)$ satisfies the linear system

$$\begin{pmatrix} D_z H(z_i,p_i) & D_p H(z_i,p_i) \\ \sigma_z^\top & \sigma_p \end{pmatrix} \begin{pmatrix} \Delta z_i \\ \Delta p \end{pmatrix} = \begin{pmatrix} -H(z_i,p_i) \\ -\sigma(z_i,p_i) \end{pmatrix}. \tag{20}$$

The way this linear system is solved depends on the size and spatial discretization of the initial PDE. For low-dimensional systems direct solvers based on the LU decomposition are used. In high-dimensional cases obtained after finite differences, elements or volumes it is still possible to use sparse direct solvers (see

for instance [38]). When the size is very large or in the case of non-sparse matrices, iterative methods are mandatory. The combination of Newton's method with iterative solvers is known as inexact Newton's methods. If the linear solvers are based on Krylov subspaces (GMRES(m), BiCGStab, FOM, TFQMR, etc., see for instance [89]) they are also called Newton-Krylov methods. The term *matrix-free methods* is also used when the linear solvers only require the user to provide products by the matrix of the system, without any explicit manipulation of its elements. GMRES(m) was used in this work. These methods do not need to be convergent for an arbitrary system, and they hardly do when looking for equilibria of discretizations of systems of parabolic PDEs. It is necessary then to use preconditioners to improve the convergence. In the case of discretizations by finite differences, volumes or elements, the use of incomplete LU decompositions usually provides efficient preconditioners, because of the sparsity of the matrices involved (see [88, 74, 94] for instance). For spectral discretizations of incompressible fluid problems, the use of the Stokes operator as preconditioner was suggested in Ref. [110] and has been used by several authors. When a pseudo-spectral method is employed, using preconditioners based on discretizations by finite differences or finite elements, on the same mesh, is a possibility (see [12]). Some iterative linear solvers require the action by the transpose of the operator. In most applications implemented using spectral methods neither the matrix of the operator nor the action by its transpose is available, although the adjoint operator has been explicitly discretized, for instance, to study energy transient growth rates [8], or to compute the coefficients of normal forms [102].

In the context of periodic orbits, other iterations based on Newton-Picard [70] and Broyden [78] algorithms have also been proposed in the past.

To study the stability of equilibria or periodic orbits it is necessary to compute the eigenvalues of maximum real part of the Jacobian at the equilibria, or the multipliers of maximum modulus of the periodic orbits. Methods based on variants of the power method are always used for high-dimensional systems. They provide the eigenvalues of maximum modulus of a given linear operator, for which only its action is required. There are mainly two options, subspace or Arnoldi's methods [87, 72]. The implementation in the ARPACK package [65, 66] of the latter was used here. In the case of periodic orbits the relevant multipliers of maximum modulus are exactly those obtained by these methods. For equlibria it is necessary to apply matrix transformations. For instance, to extract the eigenvalues of largest real part of a matrix A, those of maximum modulus of $(A-sI)^{-1}$ can be found, s being a *shift*, which can be real or complex. If μ is an eigenvalue of large modulus of $(A-sI)^{-1}$ then $\lambda = 1/(\mu - s)$ is an eigenvalues of A close to s. If λ is supposed to have a small imaginary part, then s can be real and close to zero. If the imaginary part can be large s must be complex, and it might be necessary to use several values of s to avoid missing eigenvalues. Other transformations are possible which do not require solving complex systems of linear equations (see [72] for a description of Cayley's transformation and additional information). Since we had to integrate the variational equations for the computation of periodic orbits, an exponential transformation was used to study the stability of the equilibria (see below).

3.1 Periodic orbits

Let

$$\dot{y} = f(y,p), \quad (y,p) \in \mathscr{U} \subset \mathbb{R}^n \times \mathbb{R}, \tag{21}$$

be a large-scale set of ODEs, which depends on a single parameter p. For the current problem $y = (\psi_{ij}, \Theta_{ij}, \eta_{ij})$ is the vector containing the values of the stream function ψ, the perturbation of the temperature Θ and the function η at the collocation points, the parameter p is Ra, and (21) is the system (13)-(16), (11), (12) after discretization. Let $\varphi(t,x,p)$ be the solution of (21) with initial condition x at $t = 0$ for a fixed p. It satisfies

$$D_t\varphi(t,x,p) = f(\varphi(t,x,p),p), \quad \text{and} \quad \varphi(0,x,p) = x \quad \forall p.$$

A point on a periodic orbit of the system is a solution of the system given by

$$h(\tau,x,p) \equiv x - \varphi(\tau,x,p) = 0, \tag{22}$$

$$g(x,p) = 0, \tag{23}$$

$$\sigma(\tau,x,p) = 0, \tag{24}$$

where $g(x,p) = 0$ is a phase condition to select a unique point on the orbit. A Poincaré condition was used here, i.e., the equation of a hyperplane, $g(x,p) = \langle v_\pi, x - x^* \rangle = 0$, normal to a previously computed cycle. In the formula $v_\pi = f(x^*,p^*)$, (x^*,p^*) being the last computed solution of the system during the continuation process. It could also be a physical condition able to select, locally, a unique point on each orbit. Equations (22) and (23) define a system $H(z,p) = 0$ as that of Eq. (18), with $m = n+1$ and $z = (\tau,x)$, to which continuation methods are applied. Curves $(\tau(s),x(s),p(s))$ are then obtained containing points on periodic orbits, their periods, and their corresponding parameter.

The pseudo-arclength condition now reads as

$$\sigma(\tau,x,p) = \sigma_\tau(\tau - \tau_0) + \langle \sigma_x, x - x_0 \rangle + \sigma_p(p - p_0) = 0, \tag{25}$$

which includes the period, and where, as before, (τ_0,x_0,p_0) is the extrapolated prediction during the continuation process, and $(\sigma_\tau,\sigma_x,\sigma_p)$ is an approximation of the tangent to the curve of solutions. This equation is usually computed inside any generic continuation code, so an user must only supply the evaluation of the left hand side of the two first equations of system (22)-(24). The latter can also be managed by the continuation code if it is the Poincaré condition.

Newton's iteration becomes now

$$(\tau_{i+1},x_{i+1},p_{i+1}) = (\tau_i,x_i,p_i) + (\Delta\tau_i,\Delta x_i,\Delta p_i),$$

where $(\Delta\tau_i,\Delta x_i,\Delta p_i)$ is obtained by solving the linear system

$$\begin{pmatrix} D_\tau h(\tau_i,x_i,p_i) & D_x h(\tau_i,x_i,p_i) & D_p h(\tau_i,x_i,p_i) \\ 0 & D_x g(x_i,p_i) & D_p g(x_i,p_i) \\ \sigma_\tau & \sigma_x^\top & \sigma_p \end{pmatrix} \begin{pmatrix} \Delta\tau_i \\ \Delta x_i \\ \Delta p_i \end{pmatrix} = \begin{pmatrix} -h(\tau_i,x_i,p_i) \\ -g(x_i,p_i) \\ -\sigma(\tau_i,x_i,p_i) \end{pmatrix}. \quad (26)$$

It must be stressed that even if the case of spatial discretizations by methods giving rise to a sparse Jacobian $D_y f(y,p)$, the matrix in Eq. (26) is not sparse and therefore it is not possible to apply tailored LU decompositions to solve the system (see [99] for an explanation). Each iteration of a matrix-free linear solver requires only the action of the Jacobian on vectors. One could try to approximate them by finite differences, but to enhance the convergence it is much better to compute the products of the form

$$\delta x - D_t\varphi(\tau,x,p)\delta\tau - D_x\varphi(\tau,x,p)\delta x - D_p\varphi(\tau,x,p)\delta p, \quad (27)$$
$$D_x g(x,p)\delta x + D_p g(x,p)\delta p, \quad (28)$$

for an arbitrary $(\delta\tau,\delta x,\delta p)$, by using the same spatial and temporal discretization as for the original system. Finite differences can be used just to check the right calculation of the action by the Jacobian in complicated two- and three-dimensional problems.

The evaluation of the product (28) is straightforward, and the second term of (27) is $D_t\varphi(\tau,x,p)\delta\tau = f(y(\tau),p)\delta\tau$, with $y(\tau)=\varphi(\tau,x,p)$. The matrix product $D_x\varphi(\tau,x,p)\delta x + D_p\varphi(\tau,x,p)\delta p$ can be computed by integrating a first variational equation.

Let us suppose that x and p are fixed, and let us name $y(t)=\varphi(t,x,p)$ and $y_1(t) = D_x\varphi(t,x,p)\delta x + D_p\varphi(t,x,p)\delta p$, then y_1 satisfies

$$\dot{y}_1 = D_y f(y,p)y_1 + D_p f(y,p)\delta p \quad \text{and} \quad y_1(0)=\delta x,$$

because $\varphi(0,x,p)=x$. Consequently, by integrating a time τ the system

$$\begin{aligned} \dot{y} &= f(y,p) \\ \dot{y}_1 &= D_y f(y,p)y_1 + D_p f(y,p)\delta p \end{aligned}$$

with initial conditions $y(0)=x, y_1(0)=\delta x$, the sum $D_x\varphi(\tau,x,p)\delta x + D_p\varphi(\tau,x,p)\delta p = y_1(\tau)$ is obtained.

Taking into account that Ra will be used as continuation parameter, the action of $(D_\tau h(\tau,x,p), D_x h(\tau,x,p)\ D_p h(\tau,x,p))$ on $(\delta\tau,\delta x,\delta p)$ is obtained from the first variational equations of system (13-15), which for (ψ_1,Θ_1,η_1) and δRa are

$$\begin{aligned} \partial_t\Delta\psi_1 - J(\psi,\Delta\psi_1) - J(\psi_1,\Delta\psi) =& \mathrm{Pr}\Delta^2\psi_1 - \mathrm{RaPr}[(1+\mathrm{Se})(\partial_x\Theta_1) + \mathrm{Se}\partial_x\eta_1)] + \\ &+ \delta\mathrm{RaPr}[(1+\mathrm{Se})(1-\partial_x\Theta) - \mathrm{Se}\partial_x\eta)], \quad (29) \\ \partial_t\Theta_1 - J(\psi,\Theta_1) - J(\psi_1,\Theta) =& \Delta\Theta_1 + \partial_y\psi_1, \quad (30) \\ \partial_t\eta_1 - J(\psi,\eta_1) - J(\psi_1,\eta) =& \mathrm{Le}\Delta\eta_1 - \Delta\Theta_1, \quad (31) \end{aligned}$$

with boundary conditions

$$\psi_1 = \partial_n \psi_1 = 0 \text{ on } \partial\Omega. \tag{32}$$

$$\Theta_1 = 0 \text{ on } x = 0,1 \quad \text{and} \quad \partial_y \Theta_1 = 0 \text{ on } y = 0,\Gamma, \tag{33}$$

$$\partial_n \eta_1 = 0 \text{ on } \partial\Omega. \tag{34}$$

3.2 Fixed Points

Equilibria can be computed by the continuation methods described at the beginning of this section, applied to the equation $f(x,p) = 0$. As stated before, this requires good preconditioners to accelerate the convergence of the linear solvers. They can also be obtained with the above procedure for periodic orbits. This was done, for simplicity, in the computations of the present work. If x is an equilibrium then it also solves the equation $x - \varphi(\tau,x,p) = 0$ for any τ, which can be chosen as a characteristic known time (of the order of the period of the periodic orbits for the convection problem, for instance). Therefore it is no longer an unknown of the problem, the phase condition (23) is not needed, and the τ derivatives do not appear in the action by the Jacobian (27). The advantages, compared with the continuation methods for equilibria described for instance in Refs. [88, 29, 71], are that the same code can be used for solving cycles and steady states, and that the requirement of preconditioners is avoided. The main disadvantage is that the method is, in general, more expensive.

3.3 Stability of the periodic orbits

The leading Floquet multipliers of a periodic orbit of Eq. (21), of which a point x and its period T are known for a parameter p, were computed as the leading eigenvalues (largest modulus) of the linear map $u \to D_x\varphi(T,x,p)u$, by using the package ARPACK, which, as stated before, only requires the action of the operator on vectors to provide the eigenvalues of maximum modulus. The matrix product was computed by integrating a first variational equation. If

$$y(t) = \varphi(t,x,p) \tag{35}$$

$$y_1(t) = D_x\varphi(t,x,p)u, \tag{36}$$

then y_1 satisfies $\dot{y}_1 = D_y f(y,p)y_1$, with initial condition $y_1(0) = u$, because $\varphi(0,x,p) = x$. By integrating the system

$$\dot{y} = f(y,p) \tag{37}$$

$$\dot{y}_1 = D_y f(y,p)y_1 \tag{38}$$

a time T, with initial conditions $y(0) = x$, and $y_1(0) = u$, the product $D_x\varphi(T,x,p)u = y_1(T)$ is ready to be supplied to ARPACK. The number of multipliers used to study

the stability might depend on the branch of periodic orbits studied. The larger the number of unstable multipliers, the larger the number required to have at least an stable one. In the present study it was between 16 and 26. In some cases 22 of them were unstable.

3.4 Stability of the fixed points

The leading eigenvalues λ (largest real part) of $D_y f(x,p)$ for a fixed point x and parameter p, of the system (21) were computed as the logarithms of the leading eigenvalues $\mu = \exp(\tau\lambda)$ (largest modulus) of the map $u \to \exp(\tau D_y f(x,p))u$, by means of the ARPACK package, as before. This is an exponential transform, which maps the eigenvalues λ of $D_y f(x,p)$ of largest real part to those of largest modulus of $\exp(\tau D_y f(x,p))$.

In this case, since $y(t) \equiv x$, and then the matrix $D_y f(x,p)$ is constant, the solution of the system $\dot{y}_1 = D_y f(x,p) y_1$, with initial condition $y_1(0) = u$ is

$$y_1(t) = \exp(t D_y f(x,p))u. \tag{39}$$

The matrix product $\exp(\tau D_y f(x,p))u = y_1(\tau)$ can therefore be computed by integrating only the first variational equation for a time τ. The integration time τ has to be selected large enough to clearly separate the transformed μ to have a fast convergence of the Arnoldi's methods, but as short as possible to reduce the computational cost of the integration. The same holds when the equilibria are computed as roots of $x - \varphi(\tau,x,p) = 0$.

3.5 Numerical tests

To check the reliability of the results and the resolution needed for the calculations, the gaseous mixture of $\mathrm{Pr} = 0.683$, $\mathrm{Le} = 1.085$, $\mathrm{Se} = -0.08$ was mainly used. The stability of the basic branch of steady solutions, and of the first branch of periodic orbits bifurcated from it was computed with three meshes. Table 1 shows either three eigenvalues, λ_i, or three multipliers, μ_i, with $i = 1,3,5$, when both types of solutions are already unstable. It can be seen that a mesh of $n_x \times n_y = 40 \times 140$ is sufficient in the interval of Ra considered to have errors less than 0.5% in the values of the eigenvalues and multipliers, and that the order of the bifurcations is preserved. Some additional calculations were done for the very low parameters $\mathrm{Pr} = 0.046$, $\mathrm{Le} = 0.01$, $\mathrm{Se} = -0.01$ with the two finest meshes. It was, checked that the order of the modes that become successively unstable is the same when the number of points is increased, and that at $\mathrm{Ra} = 1.975168 \times 10^3$, which corresponds to the critical Rayleigh number, Ra_c, where the basic branch of steady solutions loses stability, the relative error of the critical frequency, ω_c, is less than 0.08%. Moreover, the

Table 1 Comparison of the real and imaginary parts of the first, third and five couples of leading eigenvalues λ^i, $i = 1,3,5$ or multipliers μ^i, $i = 1,3,5$, for a steady solution (SS) or a periodic orbit (PO) of the first branch, respectively. The parameters are $\mathrm{Ra} = 5\times10^5$, $\mathrm{Pr} = 0.683$, $\mathrm{Le} = 1.085$, $\mathrm{Se} = -0.08$.

$n_x \times n_y$	Type	$\Re(\lambda^1)$	$\Im(\lambda^1)$	$\Re(\lambda^3)$	$\Im(\lambda^3)$	$\Re(\lambda^5)$	$\Im(\lambda^5)$
32×128	SS	27.40457	$\pm$982.4450	20.53312	$\pm$908.5767	7.575618	$\pm$1208.3935
40×140	SS	27.40626	$\pm$982.4565	20.53183	$\pm$908.5863	7.603457	$\pm$1208.4059
48×152	SS	27.40630	$\pm$982.4566	20.53173	$\pm$908.5864	7.604181	$\pm$1208.4052
		$\Re(\mu^1)$	$\Im(\mu^1)$	$\Re(\mu^3)$	$\Im(\mu^3)$	$\Re(\mu^5)$	$\Im(\mu^5)$
32×128	PO	-0.1340321	$\pm$1.082737	0.3377894	$\pm$1.016788	-0.8906506	$\pm$0.5174372
40×140	PO	-0.1337884	$\pm$1.082762	0.3379647	$\pm$1.016684	-0.8905498	$\pm$0.5176271
48×152	PO	-0.1331952	$\pm$1.082919	0.3385430	$\pm$1.016476	-0.8903549	$\pm$0.5180980

relative errors of the real and imaginary parts of the third pair of eigenvalues of the spectrum are 0.8% and 0.07%, respectively. Consequently, a grid of $(40,140)$ points was used for any value of Pr.

4 Gaseous mixtures. Comparison with pure gases

4.1 Steady flows and their stability

In contrast to the studies with buoyancy number $N = -1$, as soon as the fluid is heated from the side a non-trivial steady velocity field appears in the domain. The dynamics and stability of this basic steady flow of a pure fluid of $\mathrm{Pr} = 0.683$ (PF), and the binary mixture (BM) of the parameters of the preceding section, are compared here. As for the pure gaseous fluids (see [77]), the convection in the mixture starts as a single stationary vortex filling the domain, and giving rise to a temperature gradient with comparable horizontal and vertical components close to the center of the slot. The fluid goes up near the hot side and down at the cold, developing vertical boundary layers. This basic flow, like that of the PF, is center-symmetric, i.e.,

$$(\psi,\Theta,\eta)(t,1-x,\Gamma-y) = (\psi,-\Theta,-\eta)(t,x,y), \tag{40}$$

which implies

$$(v_x,v_y)(t,1-x,\Gamma-y) = -(v_x,v_y)(t,x,y). \tag{41}$$

In general, an eigenfunction or a solution fulfilling these relations will be named symmetric. Otherwise, if

$$(\psi,\Theta,\eta)(t,1-x,\Gamma-y) = (-\psi,\Theta,\eta)(t,x,y), \tag{42}$$

(43)

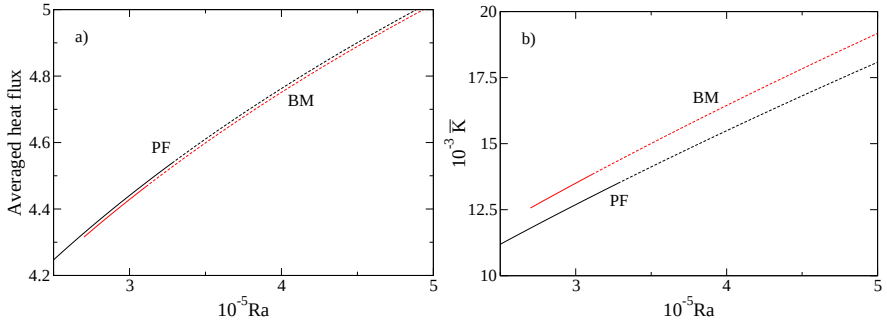

Fig. 2 Comparison of a) the averaged heat flux, and b) the kinetic energy versus the Rayleigh number of the basic steady branches of solutions and their stability for a pure fluid (PF) of Pr = 0.683 (black online), and a gaseous binary mixture (BM) of the same Pr and Le = 1.085 and Se = −0.08 (red online). Solid lines mean stable solutions, and dashed lines unstable.

which implies

$$(v_x, v_y)(t, 1-x, \Gamma - y) = (v_x, v_y)(t, x, y), \tag{44}$$

$$\tag{45}$$

it will be called antisymmetric. The symmetries of the eigenfunctions at the bifurcation points of the steady solutions determine the dynamics of the periodic flows.

Figure 2 shows the averaged heat flux through the vertical side calculated at $x = 1$ and the kinetic energy for both fluids. They are defined as

$$\overline{\partial_x T} = \frac{1}{\Gamma}\int_0^{\Gamma} \partial_x T\, dy, \qquad \text{and} \qquad \overline{K} = \frac{1}{2\Omega}\int_{\Omega} \mathbf{v}\cdot\mathbf{v}\, d\Omega. \tag{46}$$

Online, red lines refer to the mixture, and, from now on, solid lines will indicate stable solutions, and dashed unstable.

For Pr = 0.683, the steady flows lose stability through Hopf bifurcations. The double-diffusive flow becomes unstable at lower Ra, and at the onset of the oscillatory convection the period increases around 4%. The pure fluid does it at the critical Rayleigh number $\mathrm{Ra}_c = 3.279674 \times 10^5$ with critical period $\mathrm{T}_c = 7.6920 \times 10^{-3}$ while the mixture does it at $\mathrm{Ra}_c = 3.107694 \times 10^5$ with period $\mathrm{T}_c = 7.9511 \times 10^{-3}$.

Six Hopf bifurcations giving rise to stable segments on five branches of POs were found, up to $\mathrm{Ra}_c = 5 \times 10^5$, on the branch of SSs of the PF. This result is in agreement with that found in Ref. [77] for Pr = 0.71. The bifurcation points, Ra_c^i, $i = 1, 6$, together with the frequencies at the beginning of the oscillations, ω_c^i, are given in Table 2. The critical points were calculated by inverse polynomial interpolation of degrees ranging from three to ten. Concerning to the mixture, the results are shown in Table 3. From the comparison, one can state that the third and fourth bifurcations maintain the tendency of the first one, i.e., the mixture has lower Ra_c^i and ω_c^i. However, the sixth of the PF has an anomalous low frequency, like that of

Table 2 Critical Rayleigh number, Ra_c^i, $i = 1,6$, and frequency, ω_c^i, of the first six bifurcations found on the branch of steady solutions of a pure fluid of $\mathrm{Pr} = 0.683$ up to 5×10^5.

Ra_c^1	ω_c^1	Ra_c^2	ω_c^2	Ra_c^3	ω_c^3
327 967.45	816.84	329 034.81	879.78	352 428.41	972.62
Ra_c^4	ω_c^4	Ra_c^5	ω_c^5	Ra_c^6	ω_c^6
388 712.51	1085.11	433 986.87	1212.66	486 017.92	1056.29

the second and the fifth of the BM. This characteristic will be analyzed in Sect. 4.2. On the other hand, the second, fourth and sixth eigenfunctions of the PF, and the

Table 3 Critical Rayleigh number, Ra_c^i, $i = 1,6$, and frequency, ω_c^i, of the first six bifurcations found on the branch of steady solutions of the mixture up to 5×10^5. The parameters are $\mathrm{Pr} = 0.683$, $\mathrm{Le} = 1.085$, $\mathrm{Se} = -0.08$.

Ra_c^1	ω_c^1	Ra_c^2	ω_c^2	Ra_c^3	ω_c^3
310 769.39	790.23	311 887.12	730.34	331 453.40	877.09
Ra_c^4	ω_c^4	Ra_c^5	ω_c^5	Ra_c^6	ω_c^6
370 140.18	989.10	373 860.45	726.84	430 463.10	1131.35

second, third and sixth of the BM are symmetric, and the bifurcations give rise to the appearance of POs that also maintain the symmetry at any time (F-cycles). In contrast, the first, third and fifth eigenfunctions of the PF, and the first, fourth and fifth of the BM break it, although the eigenfunctions and, consequently, the bifurcated branches of POs retain the following spatio-temporal symmetry

$$(\psi, \Theta, \eta)(t, 1-x, \Gamma - y) = (\psi, -\Theta, -\eta)(t + \mathrm{T}/2, x, y), \tag{47}$$

which means

$$(v_x, v_y)(t, 1-x, \Gamma - y) = -(v_x, v_y)(t + \mathrm{T}/2, x, y). \tag{48}$$

Therefore, the POs arising at these bifurcation points are symmetric cycles (S-cycles). Advancing half a period in time is equivalent to applying the transformation (40). This property allows to halve the computational cost of the time integration during the continuation process, and to almost halve the time needed to obtain these branches.

A comparison of the steady velocity field and the contour plots of the temperature of both fluids reveals that the double diffusion together with the Soret effect does not change the main behavior of the gaseous mixtures of negative separation ratio of order 10^{-2}. It becomes determined mainly by Pr.

4.2 Periodic orbits and their stability

The branches of POs and their spectra for the PF and the BM have been calculated from the bifurcation points up to $\mathrm{Ra} = 5 \times 10^5$, or up to the points where the multipliers detach definitively from the unit circle (this will be the procedure along the present study). In this case, the bifurcations found are of Neimark-Sacker type. Either in the PF or in the BM, only the first branch of periodic solutions is stable from the bifurcation point where they arise. Each of the following has, initially, a pair of complex-conjugate multipliers outside the unit circle more than the preceding. This means, for instance, that the fifth has, at its origin, four pairs of unstable multipliers. However, from the second to the fifth branch for the PF and to the fourth for the BM, they are very close to the unit circle, and when Ra is increased they move back into it, stabilizing the cycles.

Table 4 contains the stability interval of each of the POs found. In the Table Ra_c^s means the critical Rayleigh number where the orbits stabilize, and Ra_c^d where they destabilize. The corresponding periods are T^s and T^d, respectively. The third branch of POs of the pure fluid stabilizes at $\mathrm{Ra}_c = 3.6076 \times 10^5$ with period $\mathrm{T} = 6.3790 \times 10^{-3}$, and loses stability at $\mathrm{Ra}_c = 4.341 \times 10^5$ with period $\mathrm{T} = 5.683 \times 10^{-3}$ when the first pair of leading multipliers getting into the unit circle gets out. The modulus of the same multipliers decrease again stabilizing the branch of POs at $\mathrm{Ra}_c = 4.504 \times 10^5$ with period $\mathrm{T} = 5.560 \times 10^{-3}$. Finally, the POs become unstable at $\mathrm{Ra}_c = 5.1549 \times 10^5$ with period $\mathrm{T} = 5.2090 \times 10^{-3}$. Something similar happens with the second branch of the BM. It gains stability at $\mathrm{Ra}_c = 3.2221 \times 10^5$ with period $\mathrm{T} = 8.469 \times 10^{-3}$, and loses it at $\mathrm{Ra}_c = 3.2941 \times 10^5$ with period $\mathrm{T} = 8.380 \times 10^{-3}$. The short stability interval is due to the only pair of multipliers that initially has modulus larger than one. It gets into the unit circle, and quickly moves out. The branch regains stability at $\mathrm{Ra}_c = 4.0477 \times 10^5$ with period $\mathrm{T} = 7.6245 \times 10^{-3}$ when the same multipliers become stable. Finally another different pair cross the unit circle at $\mathrm{Ra}_c = 4.1703 \times 10^5$ with period $\mathrm{T} = 7.5275 \times 10^{-3}$ and destabilizes the orbit. A plausible explanation of the origin of the short interval of stability of the second branch of POs of the BM will be given later. The sixth branch of the pure fluid, and the fifth of the mixture never gain stability in the interval considered.

The movies of the time evolution of the POs of the BM show that for $\mathrm{Pr} = 0.683$ the boundary layers are much more stable than for the pure fluid of $\mathrm{Pr} = 0.71$ studied in Ref. [77] (see below).

5 Binary mixtures

5.1 Steady solutions and their instability

The basic branches of SSs of the four BMs mentioned in Sect. 2 are shown in Fig. 3. It shows the averaged heat flux through the vertical section $x = 1$, and the kinetic

Table 4 Critical Rayleigh number and period bounding the interval of stability of the branches of periodic orbits bifurcated from the steady state in a pure fluid and a binary mixture, both of Pr = 0.683. The superscripts s and d mean stabilize and destabilize, respectively. The other parameters of the mixture are Le = 1.085, Se = −0.08.

Branch	Type	$10^{-5}\mathrm{Ra}_c^s$	$10^3\mathrm{T}_c{}^s$	$10^{-5}\mathrm{Ra}_c^d$	$10^3\mathrm{T}_c{}^d$
1	PF	3.2797	7.6920	3.3322	7.6311
2	PF	3.2934	7.1383	3.7804	6.6369
3	PF	3.6076	6.3790	4.341	5.683
3	PF	4.504	5.560	5.1549	5.2090
4	PF	4.0708	5.6377	4.4724	5.3024
5	PF	4.6619	4.9567	4.7729	4.8812
1	BM	3.1077	7.9511	4.3588	6.788
2	BM	3.2221	8.469	3.2941	8.380
2	BM	4.0477	7.6245	4.1703	7.5275
3	BM	3.4517	7.0209	4.6043	6.1247
4	BM	4.0776	6.0501	4.7073	5.6319

energy, $\overline{K}$, versus Ra. The upper figures correspond to mixtures of Pr ≈ 0.7. The main difference between them is the Lewis number. The liquid (Pr = 0.707, Le = 0.076, Se = −0.098) destabilizes before than the gas (Pr = 0.683, Le = 1.085, Se = −0.08), at $\mathrm{Ra}_c = 2.780481 \times 10^5$ with frequency $\omega_c = 715.1441$, despite its slightly higher Pr (see figure caption). Although Figs. 3a and 3b correspond to two very different fluids, there are not important differences in the values of the heat flux, and only $\overline{K}$ is slightly higher for gases. The lower Figs. 3c) and 3d) show the same plots for mixtures of Pr = 0.1, Le = 0.05 and Se = −0.05, and Pr = 0.046, Le = 0.01 and Se = −0.01. In this case, the mean values increase their difference when Ra is increased. The mixture of Pr = 0.1 loses stability at a Hopf bifurcation at $\mathrm{Ra}_c = 6.158415 \times 10^3$ with frequency $\omega_c = 18.33334$, and that of Pr = 0.046, at $\mathrm{Ra}_c = 1.975168 \times 10^3$ with frequency $\omega_c = 4.366489$.

As said before, the contour plots of the steady flows of the mixtures of Pr $\mathcal{O}(1)$ show the global circulation of the pure fluids, with tongues of cold (dense) fluid, placed near the heated side, penetrating into the hottest (lightest), located in the left and upper parts of the slot, and vice versa, at the other side, tongues of hot (light) fluid extend to the region of coldest (densest) fluid (see Fig. 4a-d). The concentration near the center remains almost uniform, mainly for the liquid mixture.

For low Pr fluids the global circulation breaks down (see Fig. 4e-h), and a central and two upper and lower vortices appear in the $\Gamma = 8$ slot when the flows are stable. The hot (cold) fluid is dragged by the vortices to the center of the box in their upper (lower) part, but keeping a remnant of a x-linear temperature stratification. However the concentration behave completely different. The three vortices confine the fluid maintaining the highest concentration at the bottom, and the lowest at the top of the box. At very low Pr the concentration remains much more uniform, and wider tongues of light (dense) fluid go down (up), connecting with the neighbor vortex.

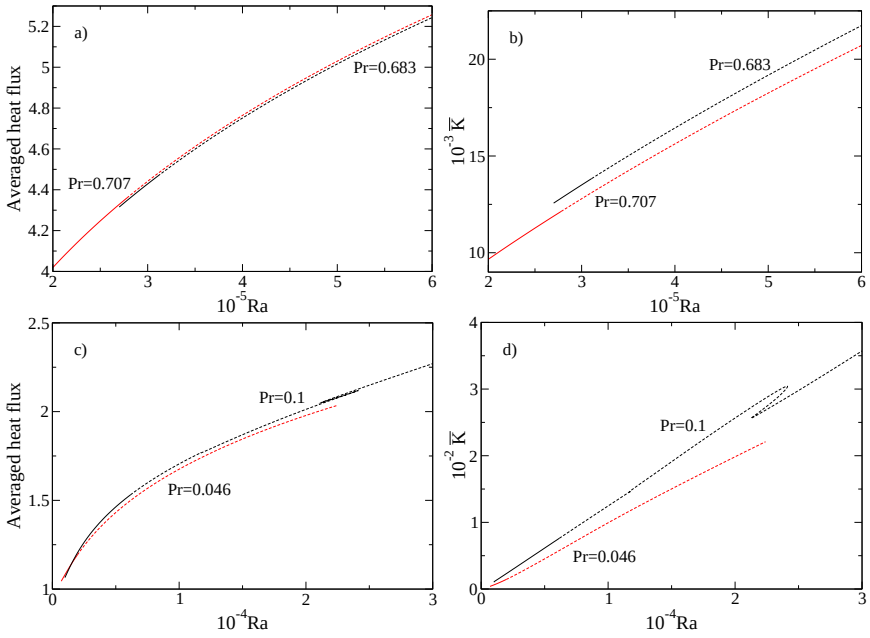

Fig. 3 Averaged heat flux and kinetic energy, $\overline{K}$ versus the Rayleigh number of steady branches of solutions and their stability. In a) and b) for $\mathrm{Pr} = 0.683$, $\mathrm{Le} = 1.085$, $\mathrm{Se} = -0.08$ and $\mathrm{Pr} = 0.707$, $\mathrm{Le} = 0.076$, $\mathrm{Se} = -0.098$, and in c) and d) for $\mathrm{Pr} = 0.1$, $\mathrm{Le} = 0.05$, $\mathrm{Se} = -0.05$ and $\mathrm{Pr} = 0.046$, $\mathrm{Le} = 0.01$, $\mathrm{Se} = -0.01$.

To evaluate the physical mechanisms contributing to the instability of the SSs, giving rise to time periodic oscillations, the total work done by the possible sources of instability, and the viscous dissipation, are calculated from the mechanical energy equation of the perturbations, as in Ref. [49]. In addition, local values of these magnitudes are also computed for the four mixtures of Fig. 3 at the first bifurcation points. The energy equation for the eigenfunction at a Hopf bifurcation can be obtained from the Navier-Stokes equation written in terms of the velocity field $\mathbf{v}$, the full temperature, T, and concentration C

$$(\partial_t + \mathbf{v}\cdot\boldsymbol{\nabla})\mathbf{v} = -\boldsymbol{\nabla}\pi + \mathrm{Pr}\,\Delta\mathbf{v} + \mathrm{Ra}\,\mathrm{Pr}\,T\mathbf{j} + \mathrm{Ra}\,\mathrm{Pr}\,\mathrm{Se}\,C\mathbf{j}, \tag{49}$$

by splitting the velocity field as $\mathbf{v} = \mathbf{v}_0 + \mathbf{v}'$, the modified pressure as $\pi = \pi_0 + \pi'$, the temperature as $T = T_0 + T'$, and the concentration as $C = C_0 + C'$, where $(\mathbf{v}_0, \pi_0, T_0, C_0)$ are the velocity, pressure, temperature and concentration fields of the SS and $(\mathbf{v}', \pi', T', C')$ their perturbations. By adding the dot product of the linearization of Eq. (49) about $\mathbf{v}_0$ times $\mathbf{v}'^*$ to its conjugated, it turns out that the kinetic energy equation of the perturbation is

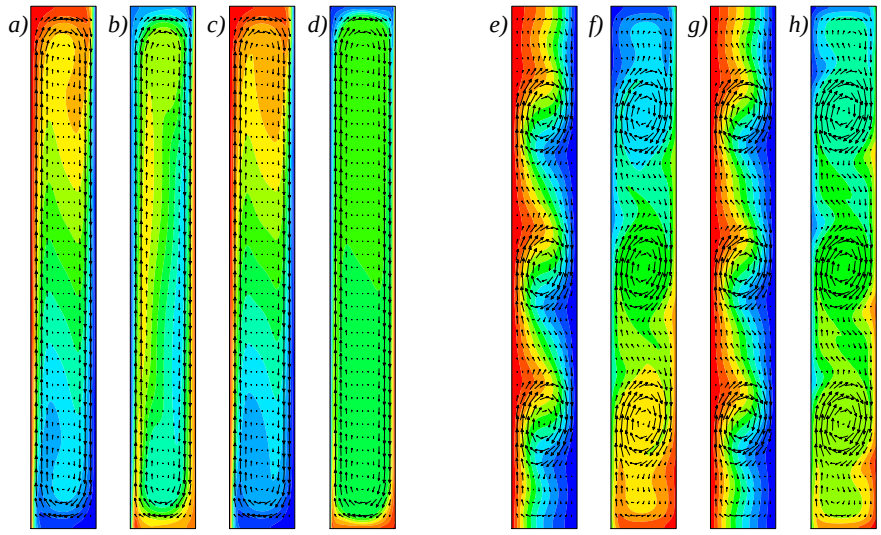

Fig. 4 Velocity field overlapped to the contour plots of a stable steady solution of a) and c) the temperature and b) and d) the concentration for $\mathrm{Ra} = 2.7 \times 10^5$, $\mathrm{Pr} = 0.683$, $\mathrm{Le} = 1.085$, $\mathrm{Se} = -0.08$ and $\mathrm{Ra} = 2.6353 \times 10^5$, $\mathrm{Pr} = 0.707$, $\mathrm{Le} = 0.076$, $\mathrm{Se} = -0.098$, and of e) and g) the temperature and f) and h) the concentration for $\mathrm{Ra} = 3.4009 \times 10^3$, $\mathrm{Pr} = 0.1$, $\mathrm{Le} = 0.05$, $\mathrm{Se} = -0.05$, and $\mathrm{Ra} = 1.8142 \times 10^3$, $\mathrm{Pr} = 0.046$, $\mathrm{Le} = 0.01$, $\mathrm{Se} = -0.01$, respectively. Dark (light) grey means low (high) temperature and concentration, except at the left side where the temperature is the highest (online, red (blue) means high (low) temperature and concentration).

$$\partial_t(\mathbf{v}' \cdot \mathbf{v}'^*/2) = \Re\big(-\mathbf{v}'^* \cdot (\mathbf{v}_0 \cdot \boldsymbol{\nabla})\mathbf{v}' - \mathbf{v}'^* \cdot (\mathbf{v}' \cdot \boldsymbol{\nabla})\mathbf{v}_0 - \mathbf{v}'^* \cdot \boldsymbol{\nabla}\pi' + \mathrm{Pr}\,\mathbf{v}'^* \cdot \Delta\mathbf{v}' + \mathbf{v}'^* \cdot \mathrm{Ra}\,\mathrm{Pr}\,T'\mathbf{j} + \mathbf{v}'^* \cdot \mathrm{Ra}\,\mathrm{Pr}\,\mathrm{Se}\,C'\mathbf{j}\big), \tag{50}$$

which is a real equation. In the case of real eigenvalues $\mathbf{v}'^* = \mathbf{v}'$, and the equation is also valid.

If the perturbation $\mathbf{v}'(\mathbf{r},t) = (v_1'(\mathbf{r}), v_2'(\mathbf{r}))\exp((\lambda + i\omega)t)$ corresponds to an eigenfunction, the left hand side of Eq. (50) gives its growth rate λ. At the bifurcation points ($\lambda = 0$), and with non-slip boundary conditions, the spatial average of this equation is just a balance between the rate of kinetic energy generated by the shear of the steady field,

$$\overline{K}_{sh} = \Re\left(-\int_\Omega v_i'^* v_j' \frac{\partial v_i}{\partial x_j}\, d\Omega \right), \tag{51}$$

by the work done by the thermal buoyancy per unit time,

$$\overline{K}_{bT} = \Re\left(\mathrm{Ra}\,\mathrm{Pr} \int_\Omega v_i'^* T' \delta_{i2}\, d\Omega \right), \tag{52}$$

by that done by the solutal buoyancy,

$$\overline{K}_{bC} = \Re\left(\mathrm{Ra}\,\mathrm{Pr}\,\mathrm{Se}\int_{\Omega} v_i'^{*} C' \delta_{i2}\, d\Omega\right), \tag{53}$$

and the rate of energy dissipated by viscosity,

$$\overline{K}_{ds} = \Re\left(-2\mathrm{Pr}\int_{\Omega} e_{ij}'^{*} e_{ij}'\, d\Omega\right), \tag{54}$$

because the rate of change of the total kinetic energy

$$\overline{K} = \left(\int_{\Omega} \frac{1}{2} v_i'^{*} v_i' d\Omega\right), \tag{55}$$

of the periodic perturbations is zero, and the preassure term of Eq. (50), and the term comming from the advection of the perturbation by the steady field can be written in flux-divergence form. Consequently, they represent spatial transport and globally neither can generate nor dissipate kinetic energy. In Eqs. (51)-(53) v_i are the components of the velocity of the steady field at the bifurcation points, v_i', T', and C' those of the critical eigenfunction, and * means complex conjugation. In Eq. (54), e_{ij}' means the strain rate tensor of the perturbation. Above but near a critical point, $\lambda > 0$ and the terms will be out of balance. However, if one of them is much larger than the rest at the onset, and almost in balance with the diffusion term, the relative weight of the terms of Eq. (50) would not differ very much from that at the transition. Consequently, this leading term will be the responsible for the instability.

When working with the mechanical energy equation one has to take into account that the term of Eq. (50) containing the laplacian does not give locally the energy dissipated by viscosity because it can be split into a transport term and the true viscous dissipation term. On the other hand, notice that Eq. (50) depends on the solution of a linearized problem, and then the results are resolution dependent because the norm of the eigenvectors does. However the normalized values $\overline{K}_{sh}/\overline{K}_{ds}$, $\overline{K}_{bT}/\overline{K}_{ds}$ and $\overline{K}_{bC}/\overline{K}_{ds}$ giving the percentage of the rate of kinetic energy generated or dissipated are independent of the grid.

Table 5 contains the values given by Eqs. (51-54) for the first six bifurcations found on the branch of SSs of the mixture of $\mathrm{Pr} = 0.683$. The total work done by the solutal buoyancy, $\overline{K}_{bC}$, contributes to the stabilization of the fluid and that done by the thermal buoyancy, $\overline{K}_{bT}$, to the destabilization, although both in a low percentage in front of the viscous dissipation, $\overline{K}_{ds}$, and of the generation of kinetic energy by shear, $\overline{K}_{sh}$. The best ratio corresponds to the kinetic energy generated by the thermal buoyancy at the fifth bifurcation, which corresponds to a 11% of the total. Table 5 also shows that there are two types of balances. The first, third, fourth and sixth have an increase of $\overline{K}_{sh}$, and a decrease of $\overline{K}_{bT}$ and of the dissipation due to $\overline{K}_{bC}$ when Ra increases. In the second and fifth bifurcations $\overline{K}_{sh}$ decreases with Ra, while $\overline{K}_{bT}$ and the absolute value of $\overline{K}_{bC}$ increase. Moreover, the values of $\overline{K}_{sh}$ are lower than for the other bifurcations, and those of $\overline{K}_{bT}$ and the dissipation due to $\overline{K}_{bC}$ higher.

By inspecting the local values of these magnitudes for the two types of balances the qualitative differences are not significant. The surface and contour plots of the

Table 5 Rate of kinetic energy generated by the shear of the SSs, $\overline{K}_{sh}$, and by the buoyancy forces, $\overline{K}_{bT}$ and $\overline{K}_{bC}$, and dissipated, $\overline{K}_{ds}$, by the perturbations at the bifurcation points. The parameters are Pr = 0.683, Se = −0.08, Le = 1.085. A means antisymmetric eigenfunction, and S symmetric. Notice that at the transition the four terms are in balance.

N bif.	Symmetry	$10^{-5}\mathrm{Ra}_c$	$\overline{K}_{sh}$	$\overline{K}_{bT}$	$\overline{K}_{bC}$	$\overline{K}_{ds}$
1	A	3.10769	22.35355	1.100092	-0.153183	-23.30045
2	S	3.11887	18.78545	1.333486	-0.182650	-19.93629
3	S	3.31453	26.25428	1.021661	-0.132786	-27.14315
4	A	3.70140	30.93177	1.001029	-0.116418	-31.81638
5	A	3.73860	15.45759	1.863884	-0.268702	-17.05277
6	S	4.30463	36.92729	0.948408	-0.105350	-37.77034

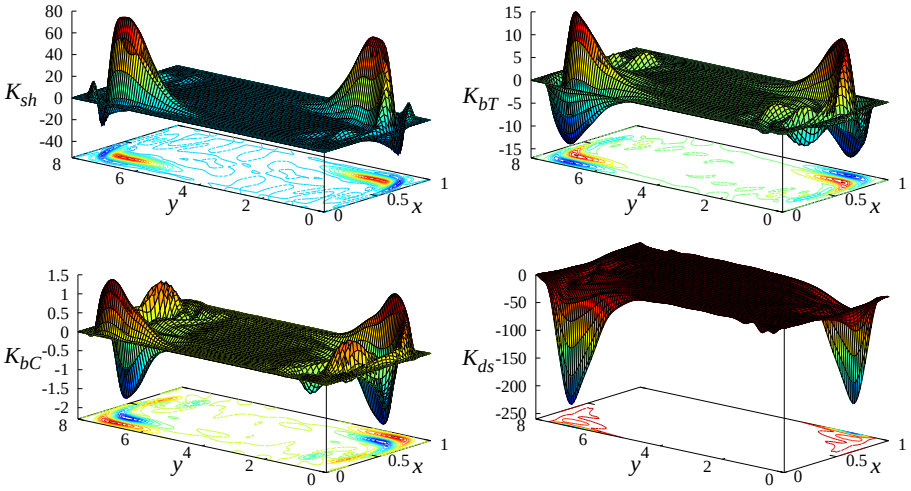

Fig. 5 Surface and contour plots of the rate of generation of kinetic energy by shear, K_{sh}, thermal buoyancy, K_{bT}, solutal buoyancy, K_{bC}, and rate of energy dissipated by viscosity, K_{ds}, at the first Hopf bifurcation for $\mathrm{Ra} = 3.10769 \times 10^5$, Pr = 0.683, Se = −0.08, Le = 1.085. The horizontal axes are not at the same scale to see the details better.

energy terms at the first and second bifurcations resemble those of Fig. 5, which correspond to the first. The generation and dissipation of K takes place, mainly, near the upper left and lower right corners of the slot. However, while the viscous dissipation happens in the boundary layers, K is generated in an elongated interior layer separated from the sides of the slot by a dissipation zone. The contribution of the concentration to stabilize the fluid takes place just where the mechanical energy by shear and by thermal buoyancy is produced, and vice versa. In this case there is also a smaller creation of net positive K parallel to the top and bottom sides. The fluid in the body of the box remains unperturbed. However, it will be seen that the two different balances have important consequences on the stability of the POs bifurcated from the SSs.

Table 6 Idem Table 5 for Pr = 0.707, Se = −0.098, Le = 0.076.

N bif.	Symmetry	$10^{-5}\mathrm{Ra}_c$	$\overline{K}_{sh}$	$\overline{K}_{bT}$	$\overline{K}_{bC}$	$\overline{K}_{ds}$
1	S	2.78048	20.63761	1.184208	0.371983	-22.19379
2	A	2.79227	24.11443	1.018217	0.465282	-25.59792
3	S	3.01721	28.13520	1.027475	0.482663	-29.64532
4	A	3.26018	32.75240	0.984464	0.534142	-34.27098
5	A	3.57044	38.38525	0.842410	0.632888	-39.86051
6	A	3.96416	45.24046	0.588907	0.788476	-46.61781

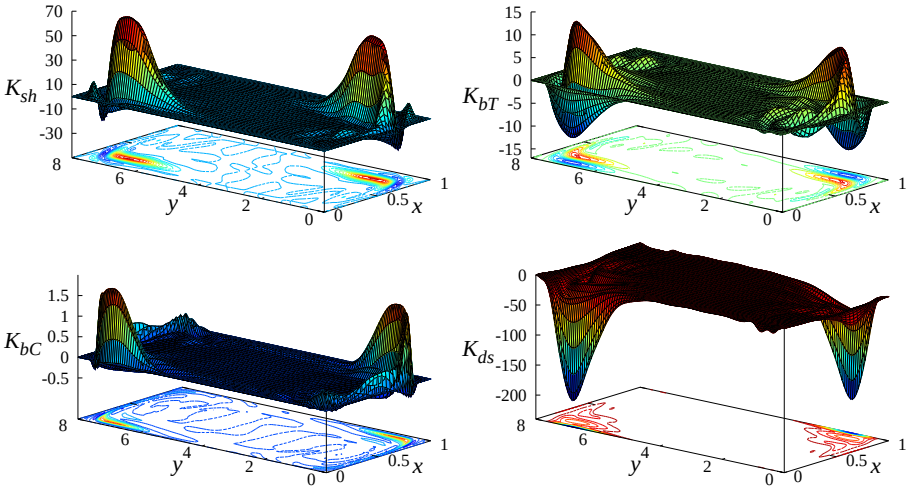

Fig. 6 Idem Fig. 5 for Ra = 2.78048×10^5, Pr = 0.707, Se = −0.098, Le = 0.076.

Table 6 shows the energy balance for the BM of Pr = 0.707. In this case the three terms contribute to the instability with an increasing weight of the generation of K by shear and by the solutal buoyancy, and a decreasing of that of the thermal buoyancy, by increasing the order of the bifurcation. However the percentage of positive work done by the buoyancies is lower than before. It barely exceeds the 7% at the first bifurcation. The surface plots of K_{sh}, K_{bT}, K_{bC} and K_{ds} of Fig. 6 resemble very much those of Fig. 5, the main difference coming from that of K_{bC}. Now the production and dissipation of energy takes place locally in the same zone as that of K_{bT}, and in addition the fluid of the lower left part of the domain, and that of the upper right part remain almost unperturbed.

Table 7 gives the balance of energies for the BM of Pr = 0.1. The lack of a clear pattern reflects very well the different types of instabilities found. The first is a Hopf bifurcation giving rise to the only branch of stable POs bifurcated from the SS. As can be seen the three terms contribute to the instability for any of the six bifurcations, and, for the first, the sum of the work done by both buoyancies arrives to 21% of the total, although $\overline{K}_{bC}$ is one order of magnitude lesser than $\overline{K}_{bT}$. The third and sixth bifurcations are of saddle-node type because of the double fold of Fig. 3c. In

Table 7 Idem Table 5, but with $10^{-2}\overline{K}_{bC}$, for Pr = 0.1, Se = −0.05, Le = 0.05.

N bif.	Symmetry	$10^{-3}\mathrm{Ra}_c$	$\overline{K}_{sh}$	$\overline{K}_{bT}$	$10^{-2}\overline{K}_{bC}$	$\overline{K}_{ds}$
1	S	6.158414	0.350650	0.090591	0.256005	-0.443803
2	A	23.60057	1.530737	0.453646	1.082218	-1.996949
3	S	24.13063	1.000072	0.256315	0.746396	-1.267125
4	A	23.80020	1.465969	0.455562	1.374090	-1.939601
5	S	22.52853	1.035993	0.101941	0.597505	-1.144304
6	S	21.25583	1.181268	0.035765	0.623779	-1.223271

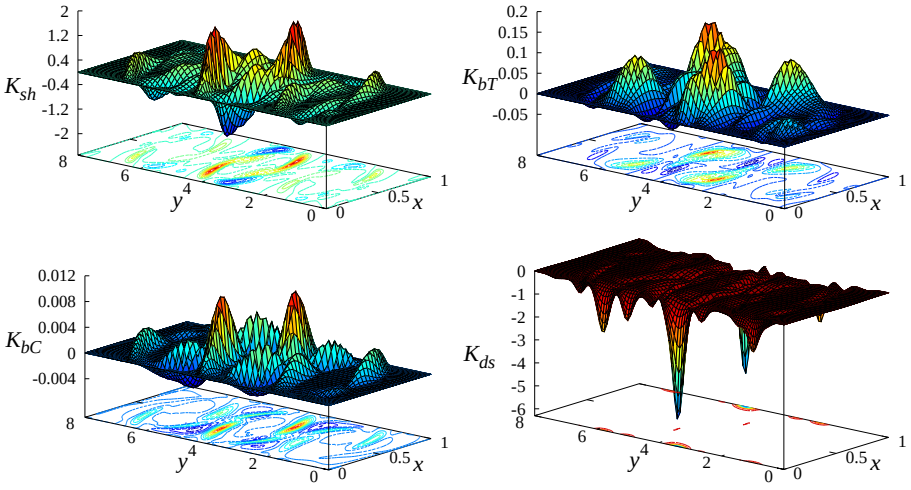

Fig. 7 Idem Fig. 5 for $\mathrm{Ra} = 6.15841 \times 10^3$, Pr = 0.1, Se = −0.05, Le = 0.05.

these bifurcations the percentage of K generated by the buoyancies decreases when Ra is decreased, but that of the shear increases by 18%. The second, fourth and five are Hopf bifurcations. The first two have the highest and similar ratios of energy supplied by the work done by the buoyancy forces, arriving to near 24%. They are similar because, as it will be seen, they give rise to a close branch of POs, starting before the first turning point and finishing after it. The fifth is a Hopf bifurcation between the two saddle-nodes. In this case the instability is due to the shear in 91%.

The surface plots of the rate of energies of Fig. 7 show that the main maxima are located in the middle of the slot around the central vortex of Figs. 4e,f. There is also a small contribution around the lateral vortices. The dissipation of energy occurs again in the boundary layer near the generation of K. A few isolated local extrema start to appear near the center for this low Pr. As for the binary mixtures of $\mathrm{Pr} = \mathscr{O}(1)$ the production and dissipation of energy is constrained to very narrow layers.

Figure 8 shows that, at the second bifurcation, the origin of the instability is much more localized in the central vortex, with a fraction of K_{sh} penetrating to the interior of the vortex. Consequently, there is also some dissipation in this zone. The upper

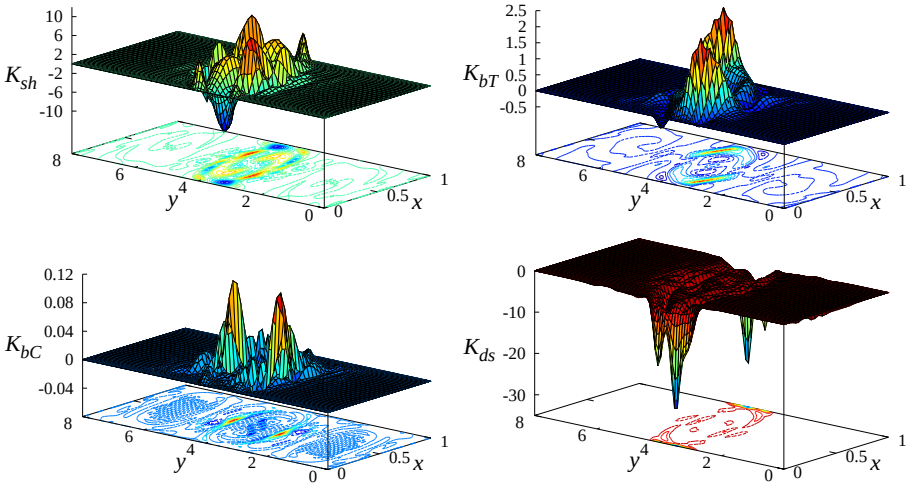

Fig. 8 Idem Fig. 7 at the second bifurcation, $\mathrm{Ra} = 2.36006 \times 10^4$.

and lower parts of the slot remain unperturbed. At the fifth bifurcation the generation of instability (not shown in a figure) takes place around all the vortices of Figs. 4e,f, with some dissipation between them, although the most important part occurs in the boundary layers, along the sides. However the thermal buoyancy force acts primary around the central vortex. In contrast, a small input of positive K due to the solutal buoyancy affects also the surroundings of the other two vortices.

Table 8 contains the same information as the preceding tables for the binary mixture of $\mathrm{Pr} = 0.046$, which corresponds to a liquid metal. As for $\mathrm{Pr} = 0.1$, the three terms contribute to the instability of the steady state, but the balance of kinetic energies is different for each of the four bifurcations considered. However, in any case the work done by the solutal buoyancy is around a 0.06%, the smallest of the mixtures studied. The first bifurcation, with the lowest relative $\overline{K}_{bT}$, near 0.5%, is the only one giving rise to a stable PO in the range of Ra considered. Its period, initially $\mathrm{T} = 1.4390$, almost triples that of the other unstable POs. At the other bifurcations the energy supplied by the shear of the steady field is reduced.

To analyze the origin of such differences, the surface and contour plots of the energies entering in the first two balances are shown in Figs. 9 and 10. The first shows that for this low Pr the generation and dissipation of energy extends along the slot for any of the terms of Eq. (50), with the extrema concentrated again around the vortices. The dissipation of energy is more important near the absolute maxima of the shear, i.e. in $(x,y) \approx (0,4)$ and $(x,y) \approx (1,4)$. The location of the maxima at the second bifurcation is completely different from the preceding cases. Although the perturbation extends along the slot, K_{sh}, K_{bT} and K_{bC} have the absolute maxima near its upper and lower sides. The dissipation behaves as usual, it is concentrated in the lateral boundary layer adjacent to the maxima with two thin interior layers. The third bifurcation (not illustrated) gives rise perturbations with the characteristics shown

Table 8 Idem Table 5, but with $10^{-2}\overline{K}_{bT}$ and $10^{-4}\overline{K}_{bC}$, for Pr = 0.046, Se = −0.01, Le = 0.01.

N bif.	Symmetry	$10^{-3}\mathrm{Ra}_c$	$\overline{K}_{sh}$	$10^{-2}\overline{K}_{bT}$	$10^{-4}\overline{K}_{bC}$	$\overline{K}_{ds}$
1	A	1.975168	0.246070	0.114012	1.491760	-0.247364
2	S	2.833397	0.193500	2.279006	0.813263	-0.216388
3	A	3.050286	0.203243	2.121481	0.991435	-0.224573
4	S	3.491323	0.260762	3.096843	1.811358	-0.292092

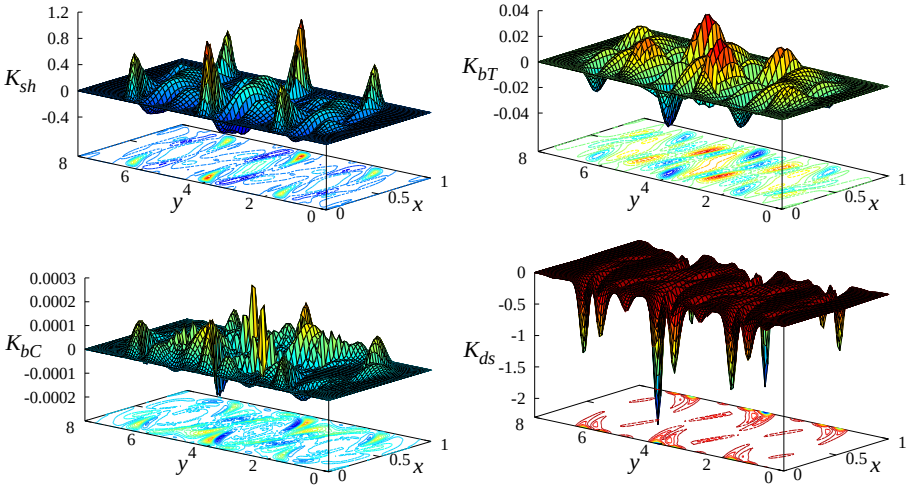

Fig. 9 Idem Fig. 5 for $\mathrm{Ra} = 1.97517 \times 10^3$, Pr = 0.046, Se = −0.01, Le = 0.01.

in Fig. 10, but with a flatter central part. Finally, the surface plots of the fourth (neither shown) displays most of the variation of the kinetic energy close to the center of the box, as the first, along two slim bands located at $y \approx 3.5$ and $y \approx 4.5$. The perturbations outside this region are much less important.

As a summary of the bifurcations analyzed, either of Hopf or real type, it is possible to state that the main source of the instabilities is the shear of the steady field. The work done by the thermal and solutal buoyancies is at most the 25% of the total contribution, and the work done by the solutal buoyancy can even help the viscous dissipation to stabilize the fluid in gases, although in a small percentage. The perturbations of the steady field are predominantly located in thin layers around the vortices, and the dissipation in the lateral boundary layers. Moreover, no relation has been found between the symmetries of the perturbations, and their energy balances and positions in the slot. The location of the generation of kinetic energy determines the features of the oscillations.

A. Y. Gelfgat and S. Molokov studied in Ref. [40] the instability at Hopf bifurcations in a quasi-two-dimensional convection problem, derived from a three-dimensional laterally heated box in a strong magnetic field normal to the main circulation, under another point of view. They stated that the averaged complex kinetic energy equation, namely that obtained by integrating over the volume the dot

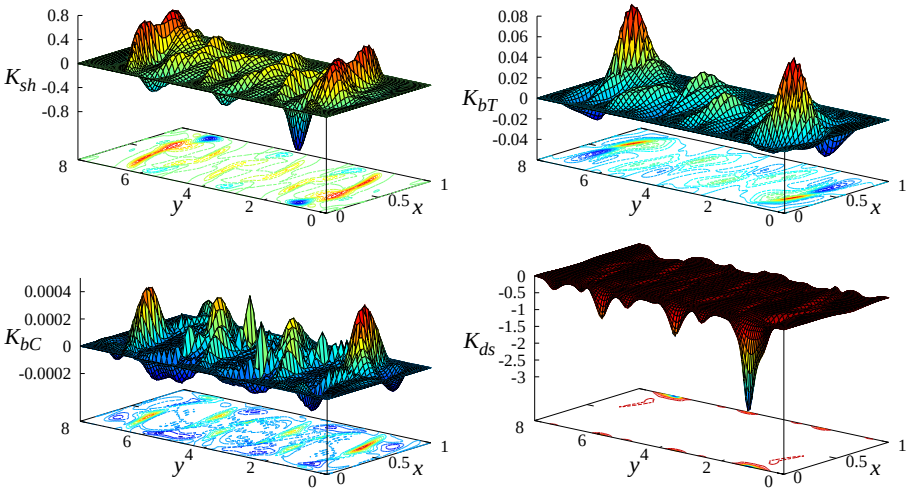

Fig. 10 Idem Fig. 9 at the second bifurcation, $\mathrm{Ra} = 2.83339 \times 10^3$.

product of the complex eigenvalue equation at the bifurcation times the conjugated eigenfunction, cannot be directly used to this purpose because the averaged complex transport terms do not vanish, as happens for real perturbations. By using the Helmholtz decomposition they first separated, if necessary, the potential part of each term of the momentum equation (which globally does not transfer energy to the perturbation) from the divergent-free part. Then, they compared the imaginary and pure real parts of the dot products of the latter with the eigenfunctions, in order to find out which contour plots of the divergent-free parts looked like those of the eigenfunctions. In this way they determined which term was responsible for the oscillations, and showed that the terms coming from the transport of momentum by the steady field were important when the perturbations grow up in the boundary layers. For instabilities developing in the bulk of the fluid this term is much less important than the shear production.

In the preceding analysis the surface plots of the shear and the buoyancies might include the potential parts, but as can be seen in the contour plots of Figs. 11a-d, showing the kinetic energy of the perturbations, their maxima are located where the rate of production (or dissipation) of this energy by shear takes place. Consequently, in this case, it has not been necessary to extract the divergence-free term to compare with the eigenfunction. The first two plots correspond to a boundary layer instability, and must be compared with the first plot of Figs. 5 and 6, and the two other to the bulk instabilities showed in the first plot of Figs. 7 and 9.

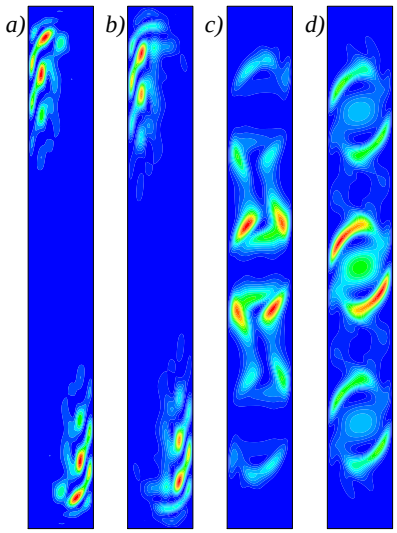

Fig. 11 Contour plots of the kinetic energy, K, of the eigenfunction at the points where the steady branches lose stability for a) $\mathrm{Pr} = 0.683$, $\mathrm{Se} = -0.08$, $\mathrm{Le} = 1.085$ at $\mathrm{Ra}_c = 3.10769 \times 10^5$, b) $\mathrm{Pr} = 0.707$, $\mathrm{Se} = -0.098$, $\mathrm{Le} = 0.076$ at $\mathrm{Ra}_c = 2.78048 \times 10^5$, c) $\mathrm{Pr} = 0.1$, $\mathrm{Se} = -0.05$, $\mathrm{Le} = 0.05$ at $\mathrm{Ra}_c = 6.15841 \times 10^3$, and d) $\mathrm{Pr} = 0.046$, $\mathrm{Se} = -0.01$, $\mathrm{Le} = 0.01$ at $\mathrm{Ra} = 1.97517 \times 10^3$. The background means $K = 0$, and the dark grey spots are the maxima of K (online, red means maximum K and blue $K = 0$).

5.2 Periodic orbits and their stability

In order to study the result of the above instabilities, the branches and stability of the periodic orbits arising at the bifurcation points of the steady states have been calculated following the methods described in Sect. 3.

5.2.1 Moderate Prandtl numbers

In the case of the binary mixtures of $\mathrm{Pr} = \mathscr{O}(1)$ the time averaged kinetic energy and heat flux of the POs almost overlap that of the corresponding steady flow shown in Figs. 3a and 3b. Then, the bifurcation diagram of POs is illustrated by means of their period versus Ra. The leftmost point of each curve lays on the curves of the SSs.

Figure 12a shows the periods of the POs of the mixture of $\mathrm{Pr} = 0.683$, $\mathrm{Le} = 1.085$ and $\mathrm{Se} = -0.08$. In agreement with the two types of balances found in Table 5, the POs of branches labelled as 2 and 5 have two differences with respect to the others. Their periods are longer, and the branches are more unstable. These properties can be attributed to the decrease of K_{sh} at these bifurcations, mentioned before. The

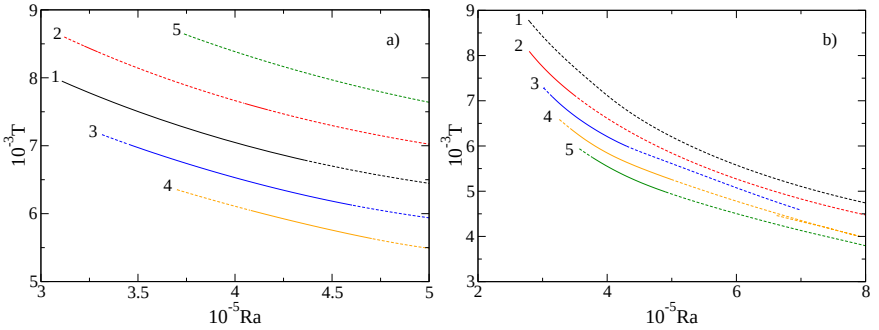

Fig. 12 Period of the branches of periodic orbits versus Ra for a) Pr = 0.683, Se = −0.08, Le = 1.085, and b) Pr = 0.707, Se = −0.098, Le = 0.076.

details on the intervals of stability of the branches of POs are included in Table 4 (BM).

Figure 12b displays the period of the branches of POs for a liquid of Pr = 0.707, Le = 0.076 and Se = −0.098. In agreement with the results of Sect. 5.1, the period of the POs is of the same order as that of the POs of Pr = 0.683 that have a very different Le and similar Se. Then it seems that what determines T is Pr. Although it cannot be appreciated in the figure the first branch is stable at the beginning, but very soon loses stability. On the contrary, the POs of the second branch are initially unstable, but becomes stable quickly. Now the branches of POs regain stability consecutively by the mechanism explained until $\overline{K}_{sh}$ doubles that of the first branch. The double line at the end of branch 4 is due to a turning point found for Ra $> 8 \times 10^5$. As happens in the convection of pure fluids of Pr ≈ 0.7 there are multiple branches of POs coexisting in the same range of parameters ([122, 77], among others). Moreover, the multistability phenomena is also present, with two, three, and even four (see for instance Fig.12a at Ra $= 4.14 \times 10^5$) stable POs in some intervals of Ra, all of them bifurcating from the same branch of steady solutions.

Snapshots of the time evolution of the velocity field, overlapped to the contour plots of the full temperature are shown in the upper row of Fig. 13 for a stable PO of the first bifurcated branch for the mixture of Pr = 0.683. The lower row depicts the concentration. This solution is an *S*-cycle, so snapshots, like for instance the third and the eighth, separated $T/2$ fulfill relations (47)-(48). By comparing the contour plots with Figs. 4a and 4b it is clear that the perturbation affects mainly the left upper and right lower parts of the slot where most of the kinetic energy is generated (see Fig 5). Instead of the waves propagating by the boundary layer described, for instance, in Ref. [77], in this case the perturbation manifests as a pumping of tongues of cold fluid up, and of hot fluid down, near the left and right boundary layers, respectively. The stratification of the fluid is weak. Sheets of high (low) concentration go up (down) by the heated (cold) side. The central part of the slot remains almost quiescent and homogeneous.

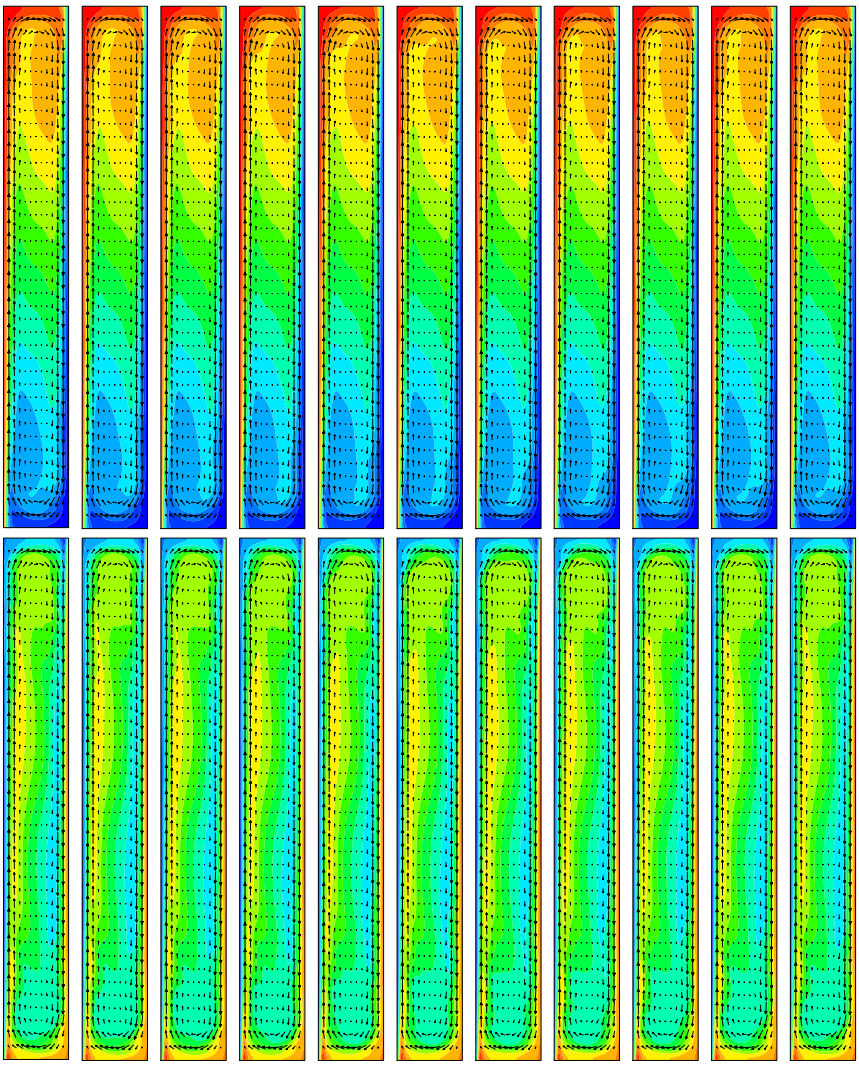

Fig. 13 Snapshots of the velocity field (arrows) superposed to the contour plots of the full temperature (upper row) and the concentration (lower row) in a period of a stable PO of the first branch. The snapshots are taken at $t = 0$, $T/10$, $T/5$, $3T/10$, $2T/5$, $T/2$, $3T/5$, $7T/10$, $4T/5$, $9T/10$, T. The parameters are $\mathrm{Ra} = 4.06017 \times 10^5$ and $\mathrm{Pr} = 0.683$, $\mathrm{Se} = -0.08$, $\mathrm{Le} = 1.085$.

The dynamics of the periodic orbits of the binary mixture of $\mathrm{Pr} = 0.707$ is similar to that shown in Fig. 13 for the temperature. The concentration remains almost homogeneous in the center of the box, as in Fig. 4d, but spots of high (low) concentration are able to rise (fall) dragged by the velocity field and to turn at the top (bottom) of the slot before diffusing into the hotter (colder) fluid. This fact is prob-

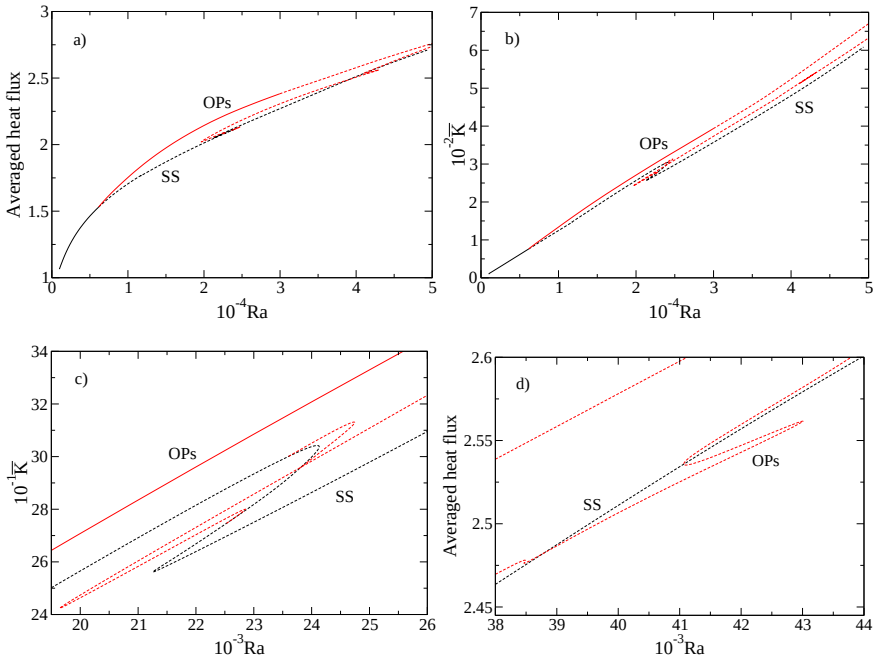

Fig. 14 a) and b) Averaged heat flux and kinetic energy versus de Rayleigh number of branches of periodic solutions and their stability for $\mathrm{Pr} = 0.1$, $\mathrm{Le} = 0.05$, $\mathrm{Se} = -0.05$. c) and d) are details of b) and a), respectively.

ably related with the positive work done by the solutal buoyancy in the corners of the slot. The boundary layers of both binary mixtures are more stable than those of a pure fluid of $\mathrm{Pr} = 0.71$. The results are coherent because the instability for the mixtures of $\mathrm{Pr} = 0.683$ and $\mathrm{Pr} = 0.707$ takes place in the same zone, and both have, near the upper left and lower right corners, a zone of negative K_{sh} and K_{bT} (see Figs. 5 and 6) that dissipate energy and help the viscous dissipation to stabilize the boundary layer. Then, it is probably that, for the parameters chosen, a narrower slot is needed to have clear trains of waves travelling along the boundary layer.

5.2.2 Low Prandtl numbers

The dynamics of the binary mixtures of low Pr has nothing to do with those of moderate Pr because the velocity field keeps a three vortex arrangement along the full period. Fig. 14 shows the bifurcation diagram of POs for the mixture of $\mathrm{Pr} = 0.1$, $\mathrm{Le} = 0.05$ and $\mathrm{Se} = -0.05$. The averaged heat flux versus Ra is shown in Figs. 14a, and 14d, and the mean kinetic energy in Figs. 14b, and 14c. Figures 14c and 14d are details of the former. The onset of the oscillations increases both quantities. This feature is understood by observing the dynamics of the orbits (see below).

The first branch of POs is supercritical, so it is stable from the bifurcation point up to a Neimark-Sacker bifurcation located at $\mathrm{Ra} = 2.9899 \times 10^4$. The period at the beginning of the oscillations is $\mathrm{T} = 0.34272$. The other two branches of POs computed never regain stability. That starting at the second Hopf bifurcation of Table 7 has a turning point at $\mathrm{Ra} = 2.4743 \times 10^4$, and connects again the steady branch at the fourth Hopf bifurcation of the same table, after its first saddle-node. The period of these orbits is lower than 0.07. The third branch followed (see details in Figs. 14c and 14d) starts at $\mathrm{Ra_c} = 2.2538 \times 10^4$, and it has two new consecutive folds at $\mathrm{Ra} = 2.2852 \times 10^4$ and $\mathrm{Ra} = 1.9644 \times 10^4$. It continues unstable up to $\mathrm{Ra} = 3.8490 \times 10^4$, where it undergoes the first of two new consecutive saddle-node bifurcations. The second turning point is located very close to the first at $\mathrm{Ra} = 3.8468 \times 10^4$. Then the branch turns down again at $\mathrm{Ra} = 4.3006 \times 10^4$, and up at 4.1067×10^4. The period of the initial PO of the third branch is 0.16919, which is of the same order as that of the first at this Ra. After the second saddle-node of the branch of SSs, there are two more Hopf bifurcations in the range of Fig. 14c, but the chance that the emerging POs become stable is very low, therefore they were not calculated.

The dynamics of the orbits along the stable branch of POs of $\mathrm{Pr} = 0.1$ is illustrated in Fig. 15. It displays as Fig. 13 the temperature in the first row, and the concentration in the second. The solutions does not break the symmetry of the SSs of Figs. 4e,f, so each snapshot fulfills the center-symmetries (40) and (41). The multi-vortex structure of the SSs of Figs. 4e,f is never broken in a period of the PO. At the beginning of the sequence, the three vortices are almost connected maintaining a temperature profile very similar to that of the SS branch. Then, they start to contract allowing that tongues of cold (hot) fluid penetrate to the interior of the slot in the upper (lower) part of the vortices, increasing the heat flux. At this point the vortices are very well defined, and allow that weak secondary vortices appear near the lids and, soon after, between them. Then all of them quickly elongate and almost reconnect closing the cycle. The time evolution of the temperature resembles that described in Ref. [98] for pure fluids of $0.3 < \mathrm{Pr} < 0.2$, but for the binary mixture of $\mathrm{Pr} = 0.1$ studied the vortices do not fully reconnect, giving rise to a global centered circulation. This fact is probably due to the lower Pr.

At first sight the vortices of the velocity field keep the concentration separated into three levels of almost constant density, with the highest concentration at the bottom. However, when the vortices elongate, small tongues of higher (lower) concentration go up (down) along the boundary of the contiguous vortices, dragged by the velocity field, and mushrooms-shaped bubbles of concentration form, moving to the lids. When the vortices shrink there is some mixing and diffusion between the vortices, and the mushrooms diffuse into the surrounding fluid of different concentration. Then the vortices stretch again ending the cycle.

For lower values of Pr the heat flux and the kinetic energy decrease. Fig. 16 shows the bifurcation diagram of the first four branches of POs computed for the binary mixture of $\mathrm{Pr} = 0.046$, $\mathrm{Le} = 0.01$ and $\mathrm{Se} = -0.01$. It shows the averaged heat flux and $\overline{K}$ versus Ra. As for $\mathrm{Pr} = 0.1$ the beginning of the oscillations increases the mean heat flux, but the mean kinetic energy of the second and third

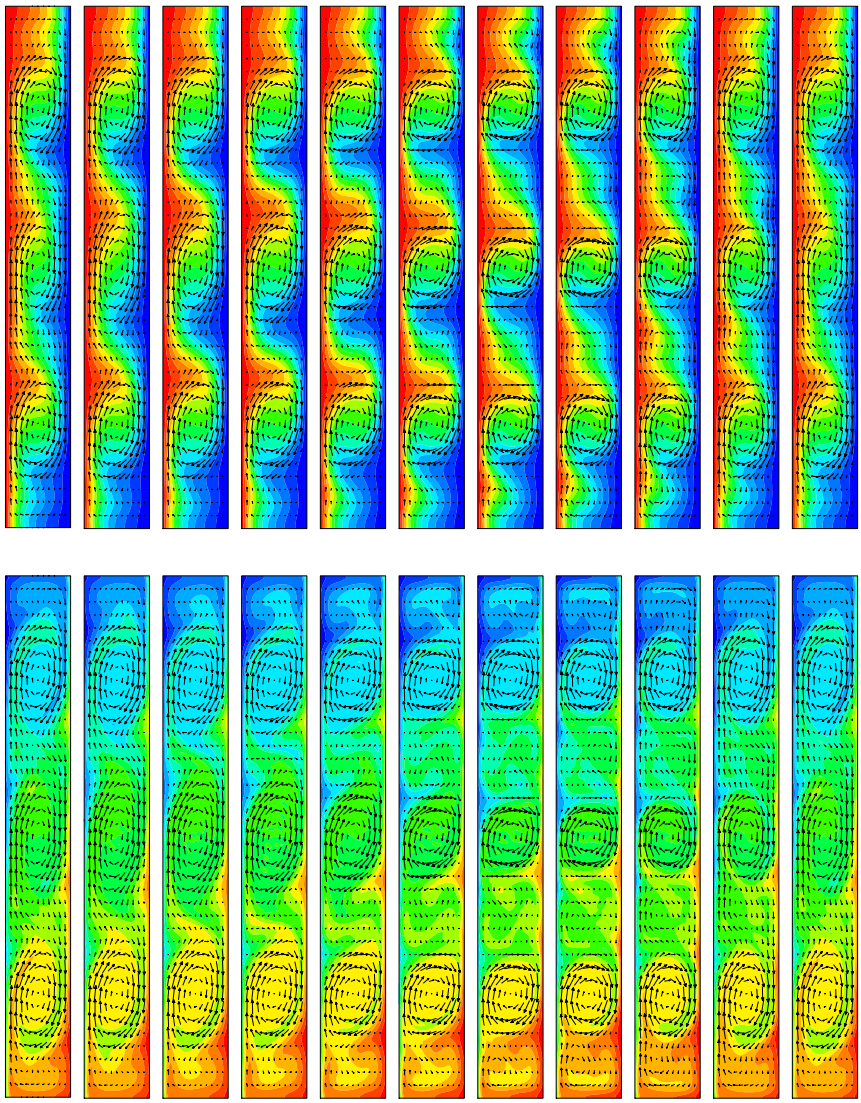

Fig. 15 Idem Fig. 13. The parameters are $\mathrm{Ra} = 1.0069855 \times 10^4$ and $\mathrm{Pr} = 0.1$, $\mathrm{Se} = -0.05$, $\mathrm{Le} = 0.05$.

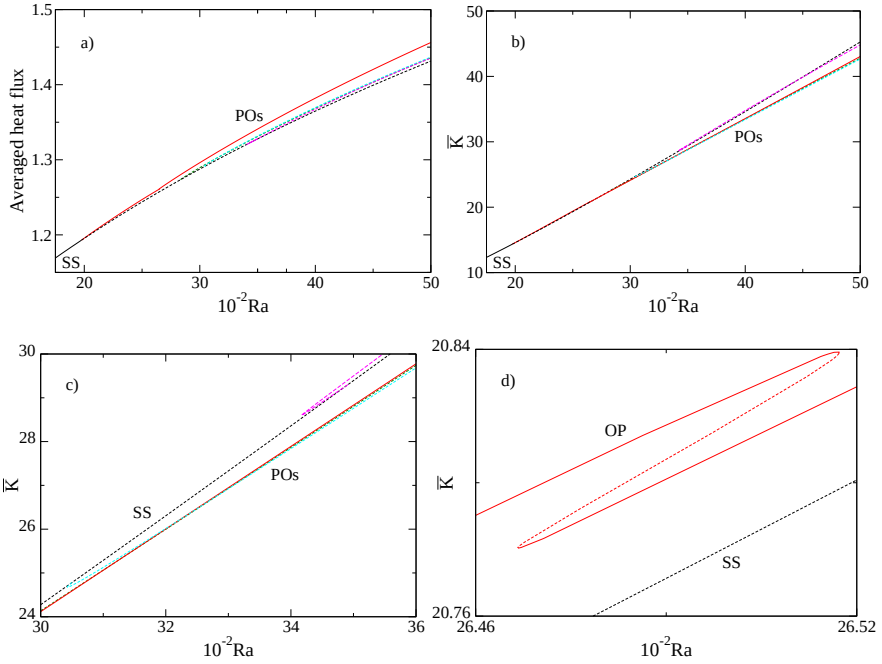

Fig. 16 a) and b) Averaged heat flux and kinetic energy versus the Rayleigh number of branches of periodic solutions and their stability for Pr = 0.046, Le = 0.01, Se = −0.01, and c) and d) details of b).

branches is lower. The first branch bifurcates at $Ra_c = 1.97517 \times 10^3$. It is supercritical, and consequently stable at onset. It undergoes two fold bifurcations in the interval $2.64666 \times 10^3 < Ra < 2.65172 \times 10^3$ (see Fig. 16d). The branch becomes unstable in the short gap between the two turnings points. The two saddle-nodes bound the only zone of coexistence of two stable solutions found at low Pr. Finally, this branch loses stability in a Neimark-Sacker bifurcation at $Ra = 6.60457 \times 10^3$. The period of the PO at the bifurcation point is T = 1.4390, and it decreases with Ra. However the period on the first branch doubles that of the others. For instance, at $Ra = 2.83350 \times 10^3$ is 1.2560, while that of the second at the bifurcation point, at $Ra = 2.83340 \times 10^3$, is 0.6121. The second branch of POs is supercritical and always unstable, like the third and fourth (see Figure 16c). The former is subcritical. It starts at $Ra = 3.05029 \times 10^3$ with period 0.5758, and it has a turning point at $Ra = 3.04277 \times 10^3$. The later bifurcates at $Ra = 3.49132 \times 10^3$ with period 0.5864, and it has a turning point at $Ra = 3.4170 \times 10^3$.

The dynamics of a stable PO at this low Pr is shown in Fig. 17. As before, the first row of snapshots corresponds to the temperature and the second to the concentration. Although in this case the first bifurcation breaks the center-symmetry of the SSs and the solution is an *S*-cycle, (compare for instance the first and sixth snapshots of the last field), the temperature behaves, along a period, like that described before

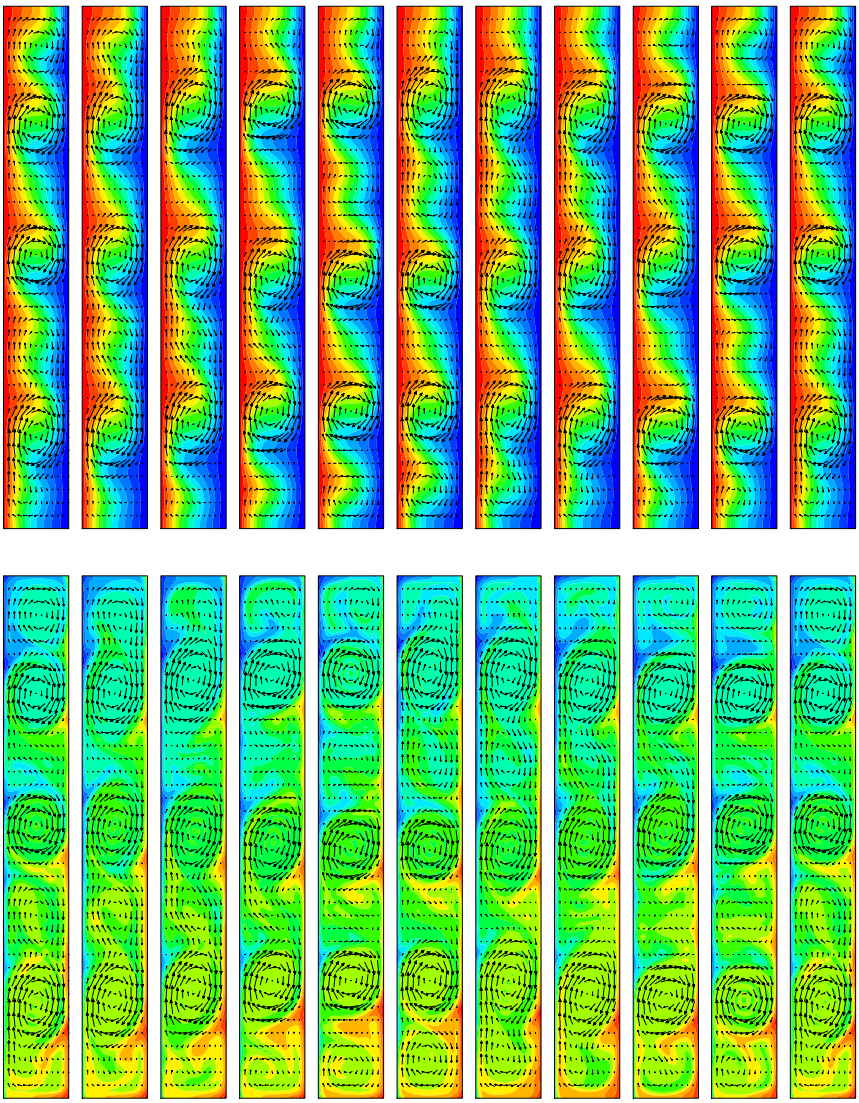

Fig. 17 Idem Fig. 13. The parameters are $\mathrm{Ra} = 4.7382217 \times 10^3$ and $\mathrm{Pr} = 0.046$, $\mathrm{Se} = -0.01$, $\mathrm{Le} = 0.01$.

for the POs of $\mathrm{Pr} = 0.1$. The main difference is that the vortices keep a rounded shape because the secondary vortices that appear either near the top and between the central and lower vortices or near the bottom and the central and upper vortices are always present and confine the main ones. Then, when the tongues of cold fluid penetrate to the interior of the slot they push slightly the hottest fluid up. In this way the center of the vortex oscillates slowly up and down.

The time evolution of the concentration allows to distinguish very well the transient vortices of the velocity field because the levels of different concentration are confined by this field. For instance, at $t = 0$ they are placed at the top and between the two lower vortices, and at $t = T/2$ at the bottom and between the two upper. The mixing by transport of fluid at different vertical levels and inside the vortices is more efficient that for fluids of $Pr = 0.1$. Some spots of high concentration are transported upwards, following trajectories external to the main vortices, to the next vortex, before diffusing. After half a period, spots of low concentration do the same in a symmetric way. When the secondary vortices develop, they open a paths that allow the fluid captured by the central vortex to travel up and down, to penetrate inside the other two main vortices forming sharp layers, or continuing by the external part up to the limits of the slot where they diffuse. Moreover, spots of high (low) concentration can also be transported to the lateral walls before diffusing.

6 Conclusions

A good performance of the Newton-Krylov techniques used here usually requires that the multipliers be tightly clustered around the origin of the complex plane. Despite the spectra of the convective solutions of the binary mixtures analyzed have several multipliers close to the unit circle (mainly when Pr is order one) the convergence of Newton's method remains quadratic, although the number of iterations needed to solve the linear systems increases. This fact has allowed to use continuation methods and stability analysis of the solutions to understand the behavior and dynamics of the stable and unstable steady and periodic flows much better than just by using direct numerical simulations. It is clear, however, that to study other invariant objects beyond quasiperiodic solutions, like strange attractors, bursts or intermittent solutions, or to compute Lyapunov exponents, the time integration cannot be substituted. However, in the case of homoclinic chains, having the possibility of computing the unstable objects allows to know which of them are visited, and drive the dynamics (see examples in Refs. [93, 33]).

From the preceding results, and their comparison with the velocity and temperature fields of pure fluids in long slots already published, some general remarks can be extracted.

- The basic steady flows always destabilize via Hopf bifurcations. The shear is the main responsible of the instability, and the work done by the two buoyancies even can help to stabilize the fluid. The main dissipation of energy takes place in the boundary layers near the maxima of the shear.
- A decrease of the generation of kinetic energy by the shear of the SSs leads to more unstable POs of higher period in gaseous mixtures.
- With $Pr \approx 0.7$ the binary mixtures have multiple stable solutions, as for the pure fluids. For $Pr \leq 0.1$ the POs are more unstable. Only one branch of stable POs bifurcating from the main branch of SSs has been found. Some branches of steady and periodic solutions are subcritical, or are folded near the bifurcation points,

but never regain stability. This means that some of the multipliers that get out of the unit circle detach quickly from it when the parameter of the continuation increases.

- The velocity and temperature fields of the binary fluids studied depend mainly on the Prandtl number. The stratification of the concentration follows closely the streamlines. Moreover, the location of the shear of the steady flows depends also on Pr. If $\mathrm{Pr} \approx 0.7$ the source of instability of the SSs is located near the corners of the slot. If $\mathrm{Pr} \leq 0.3$ (or even higher) the instability is due to the generation of kinetic energy in its center or along the body of the slot around the vortices. Depending on the location, the time periodic orbits behave as a pump of heat and concentration near the lateral sides, or as periodic oscillations of the vortices of the velocity field in the bulk of the fluid.
- For gaseous binary mixtures of $\mathrm{Pr} \approx 0.7$, and negative separation ratio, the fluid remains almost homogeneous but in the lateral boundary layers. The mean heat transported by the steady flow is almost the same as for the pure fluid, and the mean kinetic energy of the mixture increases around 10%. The result of the double diffusion and the Soret effect is to advance the onset of the oscillations, and to increase their period in comparison with that of a pure fluid of the same Prandtl number. The first branch of POs becomes stable for a larger interval of Rayleigh numbers.
- At $\mathrm{Pr} \leq 0.1$ the double diffusion stratifies the mixture forming stacked levels of decreasing concentration caught into the vortices. The oscillations increase the transport of fluid, mixing the concentration between either the main neighbor vortices or between the vortices and the top and bottom sides when the secondary vortices form. When they are destroyed, the diffusion of concentration tends to restore the levels of the steady states. The period of the POs increases by lowering Pr and decreases by increasing Ra. Moreover, with the same parameters, the period of the orbits on some branches of POs can double that of others.

`Acknowledgments` This work has been supported by Spanish MCYT/FEDER and Catalan GENCAT grants FIS2016-76525-P and 2017-SGR-1374, respectively.

References

1. Allgower, E.L., Georg, K.: Numerical Continuation Methods: An Introduction, *Computational Mathematics*, vol. 13. Springer (1990)
2. Antonijoan, J., Marqués, F., Sánchez, J.: Nonlinear spirals in the Taylor–Couette problem. Phys. Fluids **10**, 829–838 (1998)
3. Aruliah, D.A., Veen, L.V., Dubitski, A.: Algorithm 956: Pampac, a parallel adaptive method for pseudo-arclength continuation. ACM Trans. Math. Softw. **42**(1), 8:1–8:18 (2016)
4. Barkley, D., Henderson, R.D.: Floquet stability analysis of the periodic wake of a circular cylinder. J. Fluid Mech. **322**, 215–241 (1996)
5. Beaume, C., Bergeon, A., Knobloch, E.: Convectons and secondary snaking in three-dimensional natural doubly diffusive convection. Phys. Fluids **25**, 024,105–1–024,105–15 (2013)

6. Bergeon, A., Knobloch, E.: Periodic and localized states in natural doubly diffusive convection. Physica D **237**, 1139–1150 (2008)
7. Bergeon, A., Knobloch, E.: Spatially localized states in natural doubly diffusive convection. Phys. Fluids **20**, 034,102–1–034,102–8 (2008)
8. Blackburn, H.M., Barkley, D., Sherwin, S.J.: Convective instability and transient growth in flow over a backward-facing step. J. Fluid Mech. **603**, 271–304 (2008)
9. Böhmer, K., Mei, Z., Schwarzer, A., Sebastian, R.: Path-following of large bifurcation problems with iterative methods. In: E. Doedel, L.S. Tuckerman (eds.) Numerical Methods for Bifurcation Problems and Large-Scale Dynamical Systems, *IMA vol. Math. Appl.*, vol. 119, pp. 35–65. Springer, Berlin (2000)
10. Borońska, K., L.S. Tuckerman, L.: Extreme multiplicity in cylindrical rayleigh-benard convection. ii. bifurcation diagram and symmetry classification. Phys. Rev. E **81**, 036,321 (2010)
11. Brown, P.N., Saad, Y.: Hybrid Krylov methods for nonlinear systems of equations. SIAM J. Sci. Stat. Comput. **11**(3), 450–481 (1990)
12. Canuto, C., Hussaini, M.Y., Quarteroni, A., Zang, T.A.: Spectral Methods. Evolution to complex geometries and applications to Fluid Dynamics. Springer (2007)
13. Christon, M., Gresho, P., Sutton, S.: Computational Predictibility of Natural Convection Flows in Enclosures. Int. J. Numer. Methods Fluids **40**, 953–980 (2002)
14. Cliffe, K.A.: Numerical calculations of two-cell and single-cell Taylor flows. J. Fluid Mech. **135**, 219–233 (1983)
15. Cliffe, K.A.: Numerical calculations of the primary-flow exchange process in the Taylor problem. J. Fluid Mech. **197**, 57–79 (1988)
16. Cliffe, K.A., Spence, A., Taverner, S.: The numerical analysis of bifurcation problems with applications to fluid mechanics. Acta Numer. pp. 39–131 (2000)
17. COMSOL, Inc, Sweden: COMSOL Multiphysics Reference Manual, version 5.3 (2008)
18. Dankowicz, H., Schilder, F.: Recipes for Continuation. Computational Science and Engineering. SIAM (2013)
19. Davidenko, D.F.: On a new method of numerical solution of systems of nonlinear equations. Dokl. Akad. Kauk SSSR. **88**, 601–602 (1953)
20. Dembo, R.S., Eisenstat, S.C., Steihaug, T.: Inexact Newton methods. SIAM J. Numer. Anal. **19**(2), 400–408 (1982)
21. Dijkstra, H.A., Wubs, F.W., Cliffe, A.K., Doedel, E., Dragomirescu, I.F., Eckhardt, B., Gelfgat, A., Hazel, A., Lucarini, V., Salinger, A., Sánchez, J., Schuttelaars, H., Tuckerman, L., Thiele, U.: Numerical bifurcation methods and their application to fluid dynamics: Analysis beyond simulation. Commun. Comput. Phys. **15**(1), 1–45 (2014)
22. Dinar, N., Keller, H.B.: Computation of Taylor vortex flows using multigrid continuation methods. In: C.C. Chao, S.A. Orszag, W. Shyy (eds.) Recent Advances in Computational Fluid Dynamics, *Lecture Notes in Engineering*, vol. 43, pp. 191–262. Springer (1989)
23. Doedel, E.: AUTO: Software for Continuation and Bifurcation Problems in Ordinary Differential Equations. Tech. report, Applied Mathematics, California Institute of Technology, Pasadena CA (1986)
24. Doedel, E.: Lecture Notes on Numerical Analysis of Nonlinear Equations. Tech. rep., Concordia University, Canada (2007)
25. Doedel, E., Govaerts, W., Kuznetsov, Y.A.: Computation of periodic solution bifurcations in ODEs using bordered systems. SIAM J. Numer. Anal. **41**(2), 401–435 (2003)
26. Doedel, E., Tuckerman, L.S. (eds.): Numerical Methods for Bifurcation Problems and Large-Scale Dynamical Systems, *IMA Volumes in Mathematics and its Applications*, vol. 119. Springer–Verlag (2000)
27. Dorr, F.W.: The direct solution of the discrete poisson equation on a rectangle. SIAM Review **12**(2), 248–263 (1970)
28. Duguet, Y., Pringle, C.C.T., Kerswell, R.R.: Relative periodic orbits in transitional pipe flow. Phys. Fluids **20**(11), 114,102– (2008)
29. Edwards, W.S., Tuckerman, L.S., Friesner, R.A., Sorensen, D.C.: Krylov methods for the incompressible Navier-Stokes equations. J. Comput. Phys. **110**, 82–102 (1994)

30. Feigelson, R. (ed.): 50 years Progress in Crystal Growth. A reprint collection. Elsevier (2004)
31. Feudel, F., Tuckerman, L.S., Gellert, M., Seehafer, N.: Bifurcations of rotating waves in rotating spherical shell convection. Phys. Rev. E **92**, 053,015 (2015)
32. Formica, G., Arena, A., Lacarbonara, W., Dankowicz, H.: Coupling FEM with parameter continuation for analysis of bifurcations of periodic responses in nonlinear structures. J. Comput. Nonlinear Dynam. **8**(2), 021,013–8 (2012)
33. Gao, Z., Podvin, B., Sergent, A., Xin, S.: Chaotic dynamics of a convection roll in a highly confined, vertical, differentially heated fluid layer. Phys. Rev. E **91**, 013,006 (2015)
34. Gao, Z., Sergent, A., Podvin, B., Xin, S., Le Quéré, P., Tuckerman, L.S.: Transition to chaos of natural convection between two infinite differentially heated vertical plates. Phys. Rev. E **88**, 023,010 (2013)
35. Garcia, F., Net, M., García-Archilla, B., Sánchez, J.: A comparison of high-order time integrators for the Boussinesq Navier-Stokes equations in rotating spherical shells. J. Comput. Phys. **229**, 7997–8010 (2010)
36. Garcia, F., Net, M., Sánchez, J.: Continuation and stability of convective modulated rotating waves in spherical shells. Phys. Rev. E **93**, 013,119 (2016)
37. García-Archilla, B., Sánchez, J., Simó, C.: Krylov methods and test functions for detecting bifurcations in one parameter-dependent partial differential equations. BIT **46**(4), 731–757 (2006)
38. Gelfgat, A.Y.: Stability of convective flows in cavities: solution of benchmark problems by a low-order finite volume method. International Journal for Numerical Methods in Fluids **53**(3), 485–506 (2007)
39. Gelfgat, A.Y., Bar-Yoseph, P.Z., Yarin, A.L.: Stability of multiple steady states of convection in laterally heated cavities. J. Fluid Mech. **388**, 315–334 (1999)
40. Gelfgat, A.Y., Molokov, S.: Quasi-two-dimensional convection in a three-dimensional laterally heated box in a strong magnetic field normal to main circulation. Phys. Fluids **23**, 034,101–1–034,101–13 (2011)
41. Ghorayeb, K., Mojtabi, A.: Double diffusive convection in a vertical rectangular cavity. Physics of Fluids **9**(8), 2339–2348 (1997)
42. Gibson, J.F., Halcrow, J., Cvitanovic, P.: Visualizing the geometry of state space in plane couette flow. J. Fluid Mech. **611**, 107–130 (2008)
43. Goto, K., van de Geijn, R.A.: Anatomy of high-performance matrix multiplication. ACM Trans. Math. Softw. **34**(3), 1–25 (2008)
44. Govaerts, W.J.F.: Numerical Methods for Bifurcations of Dynamical Equilibria. SIAM, Philadelphia (2000)
45. Green, K.R., Van Veen, L.: Open-source tools for dynamical analysis of Liley's mean-field cortex model. J. Comput. Sci. **5**(3), 507–516 (2014)
46. Griewank, A., Reddien, G.: The calculation of Hopf points by a direct method. IMA J. Numer. Anal. **3**, 295–303 (1983)
47. de Groot, S.R., Mazur, P.: Non-Equilibrium Thermodynamics. Dover Publications, Amsterdam (1962)
48. Heil, M., Hazel, A.L.: oomph-lib – an Object-Oriented Multi-Physics Finite-Element Library. In: M. Schafer, H.J. Bungartz (eds.) Fluid-Structure Interaction, pp. 19–49. Springer (2006)
49. Henry, D., Ben Hadid, H.: Multiple flow transitions in a box heated from the side in low-Prandtl-number fluids. Phys. Rev. E **76**, 016,314 (2007)
50. Henry, D., Bergeon, A. (eds.): Continuation Methods in Fluid Mechanics, Contributions to the ERCOFTAC/EUROMECH Colloquium 383, Notes on Numerical Fluid Mechanics,. Vieweg (2000)
51. Kawahara, G., Uhlmann, M., van Veen, L.: The significance of simple invariant solutions in turbulent flows. Ann. Rev. Fluid Mech. **44**(1), 203–225 (2012)
52. Ke, H., He, Y., Liu, Y., Cui, F.: Mixture working gases in thermoacoustic engines for different applications. Int. J. Thermophys. **33**, 1143–1163 (2012)

53. Keller, H.B.: Numerical solution of bifurcation and nonlinear eigenvalue problems. In: P.H. Rabinowitz (ed.) Applications of Bifurcation Theory, pp. 359–384. Academic Press, New York (1977)
54. Keller, H.B.: Lectures on Numerical Methods in Bifurcation Theory. Tata Institute of Fundamental Research, Lectures on Mathematics and Physics. Springer-Verlag, New York (1987)
55. Kim, K.M., Witt, A.F., Gatos, H.C.: Crystal growth from the melt under destabilizing thermal gradients. J. Electrochem. Soc. **119**(9), 1218–1226 (1972)
56. Kranenborg, J.: Double-diffusive convection due to lateral thermal forcing. Ph.D. thesis, Utrecht University (1996)
57. Krauskopf, B., Osinga, H.: Computing invariant manifolds via the continuation of orbit segments. In: B. Krauskopf, H. Osinga, J. Galán-Vioque (eds.) Numerical Continuation Methods for Dynamical Systems: Path following and boundary value problems, Understanding Complex Systems, pp. 117–154. Springer-Verlag (2007)
58. Krauskopf, B., Osinga, H.M., Doedel, E.J., Henderson, M.E., Guckenheimer, J., Dellnitz, M., Junge, O.: A survey of methods for computing (un)stable manifolds of vector fields. Int. J. Bifurcation Chaos Appl. Sci. Eng. **15**, 763–791 (2005)
59. Kubíček, M., Marek, M.: Computational Methods in Bifurcation Theory and Dissipative Structures. Springer-Verlag (1983)
60. Kuznetsov, Y.A.: Elements of Applied Bifurcation Theory. Springer, Berlin (1998)
61. Lappa, M.: Thermal Convection: Patterns Evolution and Stability. Wiley, Singapore (2010)
62. Le Quéré, P.: Transition to unsteady natural convection in a tall water-filled cavity. Phys. Fluids A **2**(4), 503–515 (1990)
63. Le Quéré, P., Behnia, M.: From onset of unsteadiness to chaos in a differentially heated square cavity. J. Fluid Mech. **359**, 81–107 (1998)
64. Lee, J., Hyun, M., Kang, Y.: Confined natural convection due to lateral heating in a stably stratified solution. International Journal of Heat and Mass Transfer **33**(5), 869 – 875 (1990)
65. Lehoucq, R.B., Sorensen, D.C.: Deflation techniques for an implicitly restarted Arnoldi iteration. SIAM J. Matrix Anal. Appl. **17**, 789–821 (1996)
66. Lehoucq, R.B., Sorensen, D.C., Yang, C.: ARPACK User's Guide: Solution of Large-Scale Eigenvalue Problems with Implicitly Restarted Arnoldi Methods. Software, Environments, Tools. SIAM (1998)
67. Liu, J., Ahlers, G.: Rayleigh-bénard convection in binary-gas mixtures: Thermophysical properties and the onset of convection. Phys. Rev. E **55**, 6950–6968 (1997)
68. Lo Jacono, D., Bergeon, A., Knobloch, E.: Localized traveling pulses in natural doubly diffusive convection. Phys. Rev. Fluids **2**, 093,501–1–093,501–19 (2017)
69. Lopez, J.M., Marqués, F., Sánchez, J.: Oscillatory modes in an enclosed swirling flow. J. Fluid Mech. **439**, 109–129 (2001)
70. Lust, K., Roose, D., Spence, A., Champneys, A.: An adaptive Newton–Picard algorithm with subspace iteration for computing periodic solutions. SIAM J. Sci. Comput. **19**(4), 1188–1209 (1998)
71. Mamun, C.K., Tuckerman, L.S.: Asymmetry and Hopf bifurcation in spherical Couette flow. Phys. Fluids **7**, 80–91 (1995)
72. Meerbergen, K., Roose, D.: Matrix transformations for computing rightmost eigenvalues of large sparse non-symmetric eigenvalue problems. IMA J. Numer. Anal. **16**(3), 297–346 (1996)
73. Meyer-Spasche, R., Keller, H.B.: Computation of the axisymmetric flow between rotating cylinders. J. Comput. Phys. **35**, 100–109 (1980)
74. Molemaker, M.J., Dijkstra, H.A.: Multiple equilibria and stability of the North-Atlantic wind-driven ocean circulation. In: E. Doedel, L.S. Tuckerman (eds.) Numerical methods for bifurcation problems and large-scale dynamical systems, *The IMA volumes in Mathematics and its applications*, vol. 119, pp. 35–65. Springer (2000)
75. Moore, G., Spence, A.: The calculation of turning points of nonlinear equations. SIAM J. Numer. Anal. **17**(4), 567–576 (1980)
76. Net, M., Sánchez, J.: Continuation of bifurcations of periodic orbits for large-scale systems. SIAM J. Appl. Dyn. Syst. **14**(2), 674–698 (2015)

77. Net, M., Sánchez Umbría, J.: Periodic orbits in tall laterally heated rectangular cavities. Phys. Rev. E **95**, 023,102 (2017)
78. van Noorden, T.L., Verduyn Lunel, S.M., Bliek, A.: The efficient computation of periodic states of cyclically operated chemical processes. IMA J. Appl. Math. **68**, 149–166 (2003)
79. van Noorden, T.L., Verduyn Lunel, S.M., Bliek, A.: A Broyden rank p+1 update continuation method with subspace iteration. SIAM J. Sci. Comput. (2004)
80. Pawlowski, R.P., Shadid, J.N., Simonis, J.P., Walker, H.F.: Globalization techniques for Newton–Krylov methods and applications to the fully coupled solution of the Navier-Stokes equations. SIAM Rev. **48**, 700–721 (2006)
81. Pozzo, M., Davies, C., Gubbins, D., Alfè, D.: Transport properties for liquid silicon-oxygen-iron mixtures at earth's core conditions. Phys. Rev. B **87**, 014,110–1–014,110–10 (2013)
82. Puigjaner, D., Herrero, J., Simó, C., Giralt, F.: From steady solutions to chaotic flows in a Rayleigh–Bénard problem at moderate Rayleigh numbers. Phys. D **240**, 920–934 (2011)
83. Rheinboldt, W.C.: Numerical Analysis of Parametrized Nonlinear Equations. J. Wiley (1986)
84. Riks, E.: The application of Newton's method to the problem of elastic stability. ASME J. Appl. Mech. **39**(4), 1060–1065 (1971)
85. Roache, P.J.: Computational fluid dynamics. Hermosa Publishers Albuquerque, N.M (1972)
86. Roose, D., Hlavaček, V.: A direct method for the computation of Hopf bifurcation points. SIAM J. Appl. Math. **45**(6), 879–894 (1985)
87. Saad, Y.: Numerical Methods for Large Eigenvalue Problems. Manchester University Press, Manchester (1992)
88. Saad, Y.: Preconditioned Krylov subspace methods for CFD applications. Tech. Rep. umsi-94-171, Minnesota Supercomputer Institute, Minneapolis, MN 55415 (1994)
89. Saad, Y.: Iterative methods for sparse linear systems. PWS pub. company, New York (1996)
90. Saad, Y., Schultz, M.H.: GMRES: A generalized minimal residual algorithm for solving nonsymmetric linear systems. SIAM J. Sci. Stat. Comput. **7**, 856–869 (1986)
91. Salinger, A.G., Bou-Rabee, N.M., Pawlowsky, R.P., Wilkes, E.D., Burroughs, E.A., Lehoucq, R.B., Romero, L.A.: LOCA 1.1. Library of Continuation Algorithms: Theory and Implementation Manual. Sandia National Laboratories, Albuquerque, NM (2002)
92. Salinger, A.G., Lehoucq, R.B., Pawlowski, R.P., Shadid, J.N.: Computational bifurcation and stability studies of the 8:1 thermal cavity problem. Int. J. Numer. Methods Fluids **40**(8), 1059–1073 (2002)
93. Sánchez, J., Garcia, F., Net, M.: Computation of azimuthal waves and their stability in thermal convection in rotating spherical shells with application to the study of a double-Hopf bifurcation. Phys. Rev. E **87**, 033,014 (2013)
94. Sánchez, J., Marqués, F., López, J.M.: A continuation and bifurcation technique for Navier-Stokes flows. J. Comput. Phys. **180**, 78–98 (2002)
95. Sánchez, J., Net, M.: On the multiple shooting continuation of periodic orbits by Newton-Krylov methods. Int. J. Bifurcation Chaos Appl. Sci. Eng. **20**(1), 1–19 (2010)
96. Sánchez, J., Net, M.: A parallel algorithm for the computation of invariant tori in large-scale dissipative systems. Physica D **252**(1), 22–33 (2013)
97. Sánchez, J., Net, M.: Numerical continuation methods for large-scale dissipative dynamical systems. Eur. Phys. J. Spec. Top. **225**(13), 2465–2486 (2016)
98. Sánchez, J., Net, M.: Prandtl number dependence of convective fluids in tall laterally heated slots. European Journal of Physics Special Topics **under review** (2018)
99. Sánchez, J., Net, M., García-Archilla, B., Simó, C.: Newton-Krylov continuation of periodic orbits for Navier-Stokes flows. J. Comput. Phys. **201**(1), 13–33 (2004)
100. Sánchez, J., Net, M., García-Archilla, B., Simó, C.: Continuation of periodic orbits in large-scale dissipative systems. In: F. Dumortier, H. Broer, J. Mawhin, A. Vanderbauwhede, S.V. Lunel (eds.) Proceedings of the Equadiff-2003 Conference, pp. 625–630. World Scientific, Singapore (2005)
101. Sánchez, J., Net, M., Simó, C.: Computation of invariant tori by Newton-Krylov methods in large-scale dissipative systems. Physica D **239**, 123–133 (2010)

102. Sánchez, J., Net, M., Vega, J.: Amplitude equations close to a triple-(+1) bifurcation point of D_4-symmetric periodic orbits in $O(2)$-equivariant systems. Discrete Contin. Dyn. Syst. B **6**(6), 1357–1380 (2006)
103. Seydel, R.: Numerical computation of branch points in nonlinear equations. Numer. Math. **33**(3), 339–352 (1979)
104. Seydel, R.: Practical bifurcation and stability analysis. From equilibrium to chaos. Springer, New York (1994)
105. Shroff, G.M., Keller, H.B.: Stabilization of unstable procedures: the recursive projection method. SIAM J. Numer. Anal. **30**(4), 1099–1120 (1993)
106. Sleijpen, G.L.G., Fokkema, D.R.: BICGSTAB(L) for linear equations involving unsymmetric matrices with complex spectrum. ETNA **1**, 11–32 (1993)
107. Thurlow, M.S., Brooks, B.J., Lucas, P.G.J., Ardron, M.R., Bhattacharjee, J.K., Woodcraft, A.L.: Convective instability in rotating liquid 3he-4he mixtures. Journal of Fluid Mechanics **313**, 381–407 (1996)
108. Tiesinga, G., Wubs, F., Veldman, A.: Bifurcation analysis of incompressible flow in a driven cavity by the Newton-Picard method. J. Comput. Appl. Math. **140**(1–2), 751–772 (2002)
109. Tsitverblit, N.: Bifurcation phenomena in confined thermosolutal convection with lateral heating: Commencement of the double-diffusive region. Phys. Fluids **7**(4), 718–736 (1995)
110. Tuckerman, L.S.: Steady-state solving via Stokes preconditioning; recursion relations for elliptic operators. In: D. Dwoyer, M. Hussaini, R. Voigt (eds.) 11th Int. Conf. on Numerical Methods in Fluid Dynamics, Lecture Notes in Physics, pp. 573–577. Springer (1989)
111. Tuckerman, L.S., Barkley, D.: Bifurcation analysis for timesteppers. In: E. Doedel, L.S. Tuckerman (eds.) Numerical Methods for Bifurcation Problems and Large-Scale Dynamical Systems, *IMA Volumes in Mathematics and its Applications*, vol. 119, pp. 453–466. Springer–Verlag (2000)
112. Uecker, H., Wetzel, D., Rademacher, J.: pde2path - a matlab package for continuation and bifurcation in 2d elliptic systems. Num. Math.: Th. Meth. Appl. **7**, 58–106 (2014)
113. van Veen, L., Kawahara, G., Atsushi, M.: On matrix-free computation of 2D unstable manifolds. SIAM J. Sci. Comput. **33**(1), 25–44 (2011)
114. Viswanath, D.: Recurrent motions within plane Couette turbulence. J. Fluid Mech. **580**, 339–358 (2007)
115. Wakitani, S.: Flow patterns of natural convection in an air-filled vertical cavity. Phys. Fluids **10**(8), 1924–1928 (1998)
116. Wales, C., Gaitonde, A.L., Jones, D.P., Avitabile, D., Champneys, A.R.: Numerical continuation of high reynolds number external flows. International Journal for Numerical Methods in Fluids **68**(2), 135–159 (2012)
117. Waugh, I., Illingworth, S., Juniper, M.: Matrix-free continuation of limit cycles for bifurcation analysis of large thermoacoustic systems. J. Comput. Phys. **240**, 225–247 (2013)
118. Waugh, I.C., Kashinath, K., Juniper, M.P.: Matrix-free continuation of limit cycles and their bifurcations for a ducted premixed flame. J. Fluid Mech. **759**, 1–27 (2014)
119. Werner, B., Spence, A.: The computation of symmetry-breaking bifurcation points. SIAM J. Numer. Anal. **21**, 388–399 (1984)
120. Winters, K.H.: Oscillatory convection in liquid metals in a horizontal temperature gradient. Int. J. Numer. Methods Eng. **25**, 401–414 (1988)
121. Wriggers, P., Wagner, W., Miehe, C.: A quadratically convergent procedure for the calculation of stability points in finite element analysis. Comp. Meth. Appl. Mech. & Engng **70**(3), 329 – 347 (1988)
122. Xin, S., Le Quéré, P.: Natural-convection flows in air-filled differentially heated cavities with adiabatic horizontal walls. Numer. Heat Transfer. Part A **50**, 437–466 (2006)
123. Xin, S., Le Quéré, P.: Stability of two-dimensional (2D) natural convection flows in air-filled differentially heated cavities: 2D/3D disturbances. Fluid Dynamics Research **44**(3), 031,419 (2012)
124. Xin, S., Le Quéré, P., Tuckerman, L.: Bifurcation analysis of doubly-diffusive convection with opposing horizontal thermal and solutal gradients. Phys. Fluids **10**(4), 850–858 (1998)
125. Yahata, H.: Stability analysis of natural convection in vertical cavities with lateral heating. J. Phys. Soc. Jpn. **66**(11), 3434–3443 (1998)